Modulated, or long-periodic, magnetic structures of crystals

Yu. A. Izyumov

Institute of the Physics of Metals, Ural Scientific Center, Academy of Sciences of the USSR, Sverdlovsk
Usp. Fiz. Nauk **144**, 439–474 (November 1984)

The experimental results on modulated magnetic structures and the basic regularities of phase transitions between them are reviewed and are analyzed on the basis of the phenomenological theory of phase transitions with the use of the Ginzburg-Landau functionals for inhomogeneous distributions of the order parameter. Lists of presently known crystals, in which modulated magnetic structures have been observed, are presented and for many of them the form of these functionals, taking into account the crystalline anisotropy and the interaction with a magnetic field, is established. For systems admitting a Lifshitz invariant which is linear with respect to the gradient, a soliton picture of the structure of the incommensurate phase is established and the phase transition into the commensurate phase under the action of temperature or a magnetic field is analyzed. It is shown that this transition is accompanied by a "locking" of the wave vector to the commensurate value. For systems without Lifshitz invariants, which include most crystals with modulated structures, nonlinear equations for the distribution of the order parameter are investigated by asymptotic methods, and these solutions permit describing the entire complex of observed phenomena: the temperature and field dependence of the wave vector, the appearance of higher-order satellites in the neutron diffraction pattern, and the sequence of magnetic phases. Thus a systematic and complete exposition of the present experimental and theoretical status of long-periodic magnetic structures of crystals, such as the spiral structure, the longitudinal and transverse spin-wave structures, the fan structure, and others, is given in this review. The review is written so as to be accessible and of interest to a wide range of readers who are interested in both the theoretical and experimental aspects of the study of magnetic phase transitions in crystals.

CONTENTS

INTRODUCTION

The first modulated magnetic structure— a simple spiral (SS)—was discovered in $MnAu_2$ more than 20 years ago.[1] Following this discovery, longitudinal spin-wave (LSW) and transverse spin-wave (TSW) structures were discovered in other materials. All these materials, together with their variants, form a special class of structures, which can be regarded as a long-periodic modulation of simple magnetic structures—ferromagnetic or antiferromagnetic. The period of the modulation often varies continuously with the temperature, assuming values which are not commensurate with the period of the crystalline lattice, so that modulated, or long-periodic, structures are also called incommensurate structures. All these definitions are synonymous.

Figure 1 illustrates schematically the basic types of modulated structures, which include, in addition to those enumerated above, the following: the skewed ($\widetilde{SS}$) and ferromagnetic (FS) spirals and the fan (FAN) structure, which appears in a magnetic field. The arrows indicate the orientations of the magnetic moments (spins) of the atoms, lying in each atomic plane, perpendicular to this direction. All atomic spins are collinear; their orientation changes from one plane to another; and, in addition, in all the structures enumerated above, the phase difference between two neighboring planes is always constant, i.e., the spatial distribution of the spin density contains a single harmonic.

The $\widetilde{SS}$ and FAN structures require some explanation. It is convenient to characterize the spiral structure by the vector of the spiral **m**, oriented perpendicular to the rotational plane of the spins. If **m** is collinear with the direction of modulation, then we have an SS structure; if these two vectors are not collinear, then, by definition, we have an $\widetilde{SS}$ structure. The fan structure appears only in a magnetic field.

 0038-5670/84/110845-23$01.80

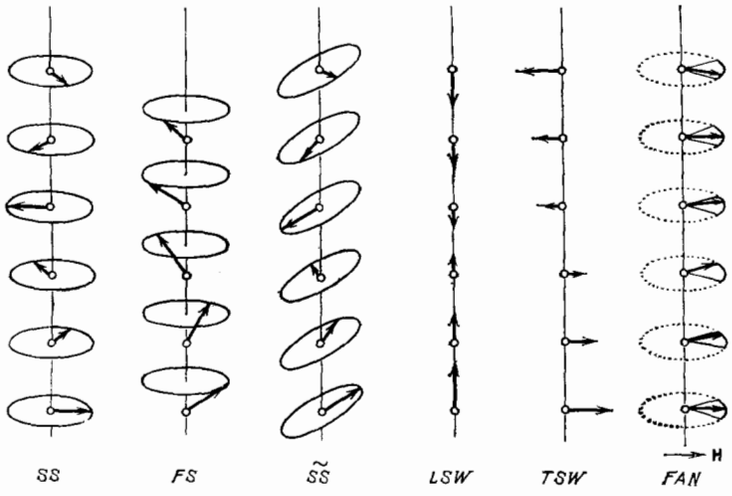

FIG. 1. Basic types of modulated magnetic structures of crystals.

Such a structure can appear in a crystal in which the SS structure occurs, if the field is applied in the plane of the spins, and it can be viewed as a modulation of the paramagnetic phase of a crystal uniformly magnetized by the field.

There are nearly 100 pure substances—metals and compounds—in which some modulated magnetic structures are observed. To them, we must add several tens of different systems of alloys, usually obtained by alloying components which themselves are ferro- and antiferromagnetic structures. Thus modulated magnetic structures are not exotic, but rather are a very common type of magnetic ordering in crystals. Although interest in them has increased appreciably in recent years in connection with the discovery of a large number of long-periodic phases in nonmagnetic, usually ferroelectric, crystals. Tens of materials in which crystalline superstructures, which are incommensurable with the period of the principal lattice and which exhibit different phase transitions between the commensurate and incommensurate phases, are known (see the reviews in Refs. 2 and 3). One of the vivid manifestations of the effects of commensurability in these materials is the appearance of the "devil's staircase" of phase transitions accompanying a change in, for example, the temperature or external field. All this makes it necessary to reexamine the problem of modulated magnetic structures of crystals in a new way and to study the entire phenomenon as a whole. To this end, we shall analyze first the results of neutron-diffraction studies of modulated magnetic phases and the basic mechanisms of the phase transitions between them under the action of temperature or an external magnetic field. Then we shall show that these mechanisms can be well understood on the basis of Landau's phenomenological theory using the Ginzburg-Landau functionals for an inhomogeneous distribution of the order parameter.

1. MODULATED MAGNETIC PHASES OF CRYSTALS

The long-periodic structures illustrated in Fig. 1 are encountered in crystals with different symmetry. A quite complete list of presently known pure substances with these structures is presented in Table I. The table indicates the space group of the crystal G and the wave vector $\mathbf{K}$. We recall that the wave vector fixes the translational properties of the structures, i.e., it permits expressing the magnetic moment $\mathbf{M}_n$ of an atom in the n-th cell of the initial crystal in terms of the vectors $\mathbf{M}_L$ given in the zeroth cell by means of the relation

$$\mathbf{M}_n = \sum_L e^{i\mathbf{K}_L \mathbf{t}_n} \mathbf{M}_L, \tag{1.1}$$

where $\mathbf{t}_n$ is the vector of translation into the nth cell. The summation extends over all the rays $\mathbf{K}_L$ of the star formed by the wave vector.

The existence of a modulated magnetic structure is inferred from the appearance of magnetic satellites in the neutron-diffraction pattern. These satellites lie near the peak of nuclear scattering, corresponding to a mode in the reciprocal lattice of the crystal, or near some symmetrical point of the reciprocal lattice, corresponding to the intial antiferromagnetic structure with wave vector $\mathbf{K}_0$. In the general case, the wave vector of the modulated structure can be represented in the form

$$\mathbf{K} = \mathbf{K}_0 + \mathbf{k}, \tag{1.2}$$

where the modulation vector $\mathbf{k}$ is much smaller than the reciprocal lattice vector.

The number of rays in the star of the wave vector $l_{\mathbf{k}}$ and, correspondingly, the number of magnetic reflections are determined by its symmetry. For example, if the vector $\mathbf{K}$ lies along a principal axis of the crystal, then its star has two rays $\mathbf{K}$ or $-\mathbf{K}$, corresponding to a pair of magnetic satellites. If $\mathbf{K}$ lies along the edge of a cube, then the star consists of six rays, corresponding to three pairs of satellites (Fig. 2). The observation of a hexad of satellites in a neutron-diffraction experiment by no means indicates that the magnetic structure is characterized by all six rays of the star. In neutron-diffraction analysis it is presumed that such a structure arises due to the presence of three types of magnetic domains in the crystal, each of which is characterized only by a pair of rays $\mathbf{K}$ and $-\mathbf{K}$. Thus it is always assumed that each domain contains a modulation in one direction only. Possible exceptions are the modulated structures in Nd and $CeAl_2$, where the

TABLE I. List of pure substances with modulated magnetic structures (**K** is the wave vector, l_k is the number of rays in the star). The references are indicated only for structures which are not described in the handbook of Ref. 5.

G	Crystal	Magnetic structure	K	l_k
C_{2h}^3	Cr_3Se_4	?	$\left[\mu\ \frac{1}{2}\ \mu\right]$	4
D_{2h}^9	$ReMn_2O_5$	SS	$\left[\frac{1}{2}\ 0\ \mu\right]$	2
	Re: Nd, Er, Tb, Y, Ho			
D_{2h}^{12}	MnOOH	TSW → SS	$[\mu_1\ 0\ \mu_3]$	4
D_{2h}^{16}	MnP, CrAs, FeAs, FeP	SS	$[00\mu]$	2
	Cr_2BeO_4	$\widetilde{SS}$	$[0\ \mu\ 0]$	2
	$KMnCl_3$	SS	$[0\ \mu\ 0]$	2
	$TbMnO_3$, Tb_3Ge	LSW	$[\mu\ 0\ 0]$	2
D_{2h}^{17}	$MnSO_4$	A → SW → SS	$[\mu\ 0\ 0]$	2
D_{2h}^{25}	Mn_3B_4	A → SS → A	$[0\ \mu\ 0]$	2
D_{2h}^{28}	$TbZn_2$	TSW	$[0\ \mu\ 0]$	2
D_{4h}^{14}	$\beta-MnO_2$, VF_2	SS	$[0\ 0\ \mu]$	2
D_{4h}^{17}	**see Table III**			
D_{4h}^{28}	$MnSn_2$	A → (A + TSW)	$[\mu\ \mu\ 0]$	4
D_{4h}^{19}	Mn_3O_4	A + SS → A	$[0\ \mu\ 0]$	4
	$TbAsO_4$ [6]	SS	$[0\ 0\ \mu]$	2
T^4	MnSi, FeG [7,8]	SS	$[\mu\ \mu\ \mu]$	8
T_h^6	$MnSe_2$	LSW	$[0\ 0\ \mu]$	6
O_h^1	$SrFeO_3$, $CaFeO_3$	SS	$[\mu\ \mu\ \mu]$	8
	ErCu, TmCu	TSW → A	$\left[\mu\ \frac{1}{2}\ 0\right]$	12
	$ErPb_3$, $HoPb_3$	LSW	$\left[0\ \mu\ \frac{1}{2}\right]$	12
	$ErTe_3$, $HoTe_3$	LSW		24
	CeB_6 [16, 15, 17]	SS	$\left[\frac{1}{4}\ \frac{1}{4}\ 0\right]$, $\left[\frac{1}{4}\ \frac{1}{4}\ \frac{1}{2}\right]$	12
O_h^5	NpAs, NpP	LSW → A	$[0\ 0\ \mu]$	6
	TbD_2	LSW + A	$[0\ 0\ \mu]$	6
	USb [9]	SW → A	$[0\ 0\ \mu]$	6
	CeSb [48–51], CeBi [52, 53]	LSW	$[0\ 0\ \mu]$	6
O_h^7	$ZnCr_2Se_4$ [10], $HgCr_2S_4$	SS	$[0\ 0\ \mu]$	6
	$TbMn_2$	$\widetilde{SS}$	$[\mu\ \mu\ 0]$	12
	$FeCr_2O_4$, $CoCr_2O_4$, $MnCr_2O_4$	FS	$[\mu\ \mu\ 0]$	12
	$CeAl_2$ [4]	LSW	$[\mu\ \bar{\mu}\ 0]$	24
O_h^9	Eu	SS	$[0\ 0\ \mu]$	6
	Cr	TSW → LSW	$[0\ 0\ \mu]$	6
C_{3i}^2	$BaCo_2(XO_4)$, X-As, P	$\widetilde{SS}$	$[\mu\ 0\ \mu_1]$	6
	$FeCl_3$	SS	$[4\mu\ \mu\ 0]$	6
	$LaLiFeO_6$ [18]	?	$[\mu\ \mu\ 0]$	6
D_{3d}^2	Cr_5S_6	A → SS	$[0\ 0\ \mu]$	2
D_{3d}^3	FeI_2, $MnBr_2$	?	$[\mu\ \mu\ \bar{\mu}]$	12
	MnI_2	SS	$[\mu_1 0\ \mu_3]$	6
D_{3d}^5	$NiBr_2$ [11]	A → SS	$\left[\mu\ \bar{\mu}\ \frac{1}{2}\right]$	6
	Re_2Fe_{17}, Re-Ce, Lu, Tm	SS → F	$[\mu\ \mu\ \mu]$	2
D_6^2	$CsCuCl_3$ [12]	SS	$\left[\frac{1}{3}\ \frac{1}{3}\ \mu\right]$	4
D_{6h}^3	CrB_2 [13]	SS	$[\mu\ \mu\ 0]$	6
	Tb_5Ge_3 [14]	SS	$[0\ 0\ \mu]$	2
D_{6h}^4	**See Table II**			

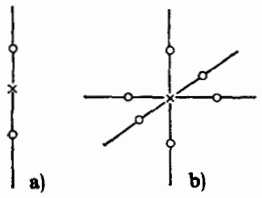

FIG. 2. Position of magnetic reflections in the case of axial (a) and cubic (b) symmetry of the wave vector.

existence of multiray (multi-**k**) structures is postulated.[4] Thus, for modulated structures, the spatial distribution of the magnetic moment is described by a particular form of the relation (1.1), which we shall write in the continuous approximation:

$$\mathbf{M}(\mathbf{r}) = \mathbf{M}e^{i\mathbf{K}\mathbf{r}} + \mathbf{M}^* e^{-i\mathbf{K}\mathbf{r}}. \quad (1.3)$$

It is evident that this relation describes an LSW or a TSW type structure if **M** is real and a spiral structure if **M** is complex.

The numerical values of the modulation parameters μ are not presented in Table I, but in all cases $\mu \ll 1$, which corresponds to long-periodic structures. As is evident from this table, modulation of the initial structures with $\mathbf{K}_0 = 0$ appears most often. Nevertheless, there are a number of examples (see also Table III) of crystals in which $\mathbf{K}_0 \neq 0$. For example, a number of compounds with the space group O_h^1 exhibit a modulation of antiferromagnetic structures with $\mathbf{K}_0 = [0\ 0\ \frac{1}{2}]$ (all wave vectors are expressed in units of $2\pi/a$, where a is the lattice constant).

The type of modulated structure is indicated in the third column of Table I; details concerning it can be found in the corresponding reference. For brevity, we primarily refer to the handbook of Ref. 5, where the required references up to 1975 can be found. If a structure is not described in this handbook, then the original sources are cited. In many cases, as is evident from the table, the modulated structure is not the only magnetically ordered phase of the crystal. It can be preceded by or can be followed by a commensurate antiferromagnetic (A) or ferromagnetic (F) structure. The corresponding phase transitions, which arise as the temperature is decreased, are marked in the table by arrows.

The table shows that there are numerous realizations of the basic types of modulated structures enumerated in Fig. 1; in addition, the symmetry of the crystal does not impose any significant restrictions on the possibility of their existence. We note that there are two large groups of isomorphic crystals (with space groups D_{4h}^{17} and D_{5h}^{4}), in which a large number of modulated phases and transitions between them is realized. Since they are very convenient for theoretical analysis, information on the modulated structures in them is given separately in Tables II and III, where the results of a symmetry analysis (see below) are also presented.

The microscopic mechanisms responsible for the modulation of magnetic structures have been known for a long time. For insulators and semiconductors, exchange interactions with different signs between the nearest-neighbor and next-to-nearest-neighbor atoms are primarily responsible for the modulation. In the case of rare-earth metals, the interaction of the magnetic order with the conduction electrons, leading to the rearrangement of the electronic states near the Fermi surface, is responsible for the modulation. For some crystals with special symmetry, the modulation is due to the nonuniform anisotropic forces of relativistic origin. The main problem to which we wish to call attention is the phase transitions between the incommensurate and commensurate structures and the response of the phases to a change in the temperature or the field.

2. BASIC EXPERIMENTAL REGULARITIES

We shall present four of them, concerning the behavior of the wave vector and of the magnetic structure in response to a change in the temperature of the field.

a) The wave vector of the modulated structure usually depends on the temperature; in addition, as T is decreased, the wave vector changes in a direction toward the point $\mathbf{K}_0$. This change can be monotonic in the range of temperatures at which the given modulated structure exists (as, for example, in the case of the spiral structure in Dy) or nonmonotonic (as in the spiral phase in Er) (Fig. 3). In the case of Er, a remarkable fact is that when the commensurate value $\mu = 1/4$ is attained, the wave vector does not change in a

TABLE II. Experimental data on magnetic structures of rare-earth metals[19] and the results of a symmetry analysis,[36] $\mathbf{m}_z = (001)$, $\mathbf{m} = (1 - i0)$, $\xi = \eta^*$.

Metal	Structure	T_c, K	K	OP, $\mathbf{K}_0 = 0$	Expression for M(z) in terms of the order parameter	Functional
Tm	LSW	57	$[00\mu]$	τ_3	$\eta\mathbf{m}_z$	1M
Ho	SS	130	$[00\mu]$	τ_9	$\eta\mathbf{m}+\xi\mathbf{m}^*$	2M ($n=6$)
	FS	19	$+\mathbf{k}=0$	$\tau_9+\tau_3$	$\eta_1\mathbf{m}_z+\eta\mathbf{m}+\xi\mathbf{m}^*$	
Tb	SS	230	$[00\mu]$	τ_9	$\eta\mathbf{m}+\xi\mathbf{m}^*$	2M ($n=6$)
			$\downarrow$			
	F	219	$\mathbf{k}=0$	τ_9		
Dy	SS	176	$[00\mu]$	τ_9	$\eta\mathbf{m}+\xi\mathbf{m}^*$	2M ($n=6$)
			$\downarrow$			
	F	88	$\mathbf{k}=0$	τ_9		
Er	LSW	84	$[00\mu]$	τ_3	$\eta_1\mathbf{m}_z$	1M
	LSW+SS	52	$[00\mu]$	$\tau_3+\tau_9$	$\eta_1\mathbf{m}_z+\eta\mathbf{m}+\xi\mathbf{m}^*$	1M+2M ($n=6$)
	FS	18	$+\mathbf{k}=0$	$\tau_3+\tau_9$		

TABLE III. Experimental data on magnetic structures in $DyAg_2$ type crystals and the results of symmetry analysis.[36]

Material	Structure	T_c, K	K	OP, K_0	Expression in terms of the order parameter	Functional
$DyAg_2$	TSW	15	$\left[\frac{1}{2}\ \frac{1}{2}\ 0\right]$ $[\mu\mu 0]$, $\mu=0{,}426$	τ_7		
	A	9,5	$\left[\frac{1}{2}\ \frac{1}{2}\ 0\right]$			
$DyAu_2$	TSW	33.8	$[\mu\mu 0]$, $\mu=0{,}411$			
	A	25.5	$\left[\frac{1}{2}\ \frac{1}{2}\ 0\right]$	τ_7	$\eta m_7 e^{iK_0 t_n}$	1M
$TbAu_2$	TSW	55	$[\mu\mu 0]$, $\mu=0{,}418-0{,}422$	τ_7		
	A	42.5	$\left[\frac{1}{2}\ \frac{1}{2}\ 0\right]$			
DyC_2	TSW	59	$[\mu\mu 0]$, $\mu=0{,}382$	τ_7		
$HoAg_2$	LSW	5.7	$[\mu\mu 0]$, $\mu=0{,}413$	τ_5 τ_7	$(\eta_1 m_5+\eta_2 m_7)e^{iK_0 t_n}$	
	LSW+TSW	4,7				
$HoAu_2$	TSW	9.2	$[\mu\mu 0]$, $\mu=0{,}406$	τ_3	$(\eta_1 m_3+\eta_2 m_7)e^{iK_0 t_n}$	
	TSW+A	7.8	$\left[\frac{1}{2}\ \frac{1}{2}\ 0\right]$	τ_7		
$ErAu_2$	TSW	6.7	$[\mu\mu 0]$, $\mu=0{,}4$	τ_3	$(\eta_1 m_3+\eta_2 m_5)e^{iK_0 t_n}$	1M+1M
	TSW+A	4.0	$\left[\frac{1}{2}\ \frac{1}{2}\ 0\right]$	τ_5		
$ErAg_2$	$\widetilde{SS}$	5.2	$[\mu\mu 0]$, $\mu=0{,}407$	$\tau_3+\tau_5$		
	$\widetilde{SS}$+A	3.5	$\left[\frac{1}{2}\ \frac{1}{2}\ 0\right]$, $[\mu\mu 0]$	$\tau_3+\tau_5$	$(\eta_1 m_3+\eta_2 m_5)e^{iK_0 t_n}$	
HoC_2	$\widetilde{SS}$	26	$[\mu 01]^{[001]}$, $\mu=1/8$	τ_9	$\eta m_9 e^{iK_0 t_n}+\xi m_9^* e^{-iK_0 t_n}$ $\xi=\eta^*$	$2M_2$
TbC_2	$\widetilde{SS}$	66	$[\mu 01]$, $\mu=1/8$	τ_9		
$MnAu_2$ [1]	SS	370	$[0\mu 0]^{[000]}$, $\mu=0$, $1/2-0{,}125$	τ_9	$\eta m_9+\xi m_9^*$	2M ($n=4$)
$PrCo_2Ge_2$ [38]	LSW	27	$[00\mu]$, $\mu=0{,}058$	τ_3	$\eta(001)$	1M

fixed temperature interval. This phenomenon is called locking of the wave vector. Such commensurability effects are also observed in a number of nonmagnetic modulated phases (see the review of Ref. 3) as well as in some other magnetic materials. The temperature at which stabilization of the wave vector of the commensurate phase appears is the point of the phase transition between the incommensurate (IC) and commensurate (C) phases.

Figure 4 shows other examples of a nonmonotonic change of the wave vector in magnetic crystals, which, possibly, correspond to locking of the wave vector. For magnetic systems, such situations are relatively rare. Nevertheless, a simple temperature-induced change in the wave vector is a very common phenomenon, its scale is often small (a change in **K** of the order of several percent), and it often terminates by a jump of the vector **K** to the value $\mathbf{K}_0$ at the point of the first-order phase transition from the modulated phase into the commensurate ferro- or antiferromagnetic phase. A typical example is the phase transition TSW→A in $TbAu_2$, in which a change in the wave vector of the form $[\mu\mu 0]$→[1/2 1/2 0] occurs (Fig. 5, Table 3).

b) Multiple harmonics. In the presence of a temperature-induced change of the wave vector, higher-order magnetic satellites, corresponding to multiple harmonics in the spatial distribution of the magnetic moment, are sometimes observed. Thus fifth- and seventh-order satellites are ob-

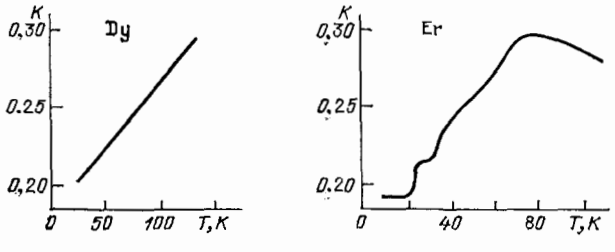

FIG. 3. Two types of variations of the wave vector with temperature in spiral phases of Dy and Er.

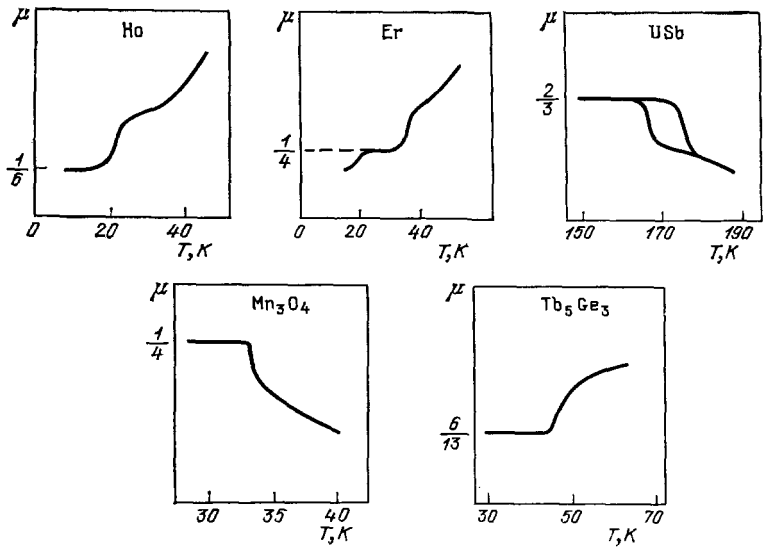

FIG. 4. Nonmonotonic variations with temperature of the wave vector in crystals.

served in the SS phase of Ho. Higher-order satellites are especially distinct in Er, where a cascade of phase transitions is observed:

$$\mathrm{LSW}\,(T_1 = 80\,\mathrm{K}) \to \mathrm{CS}\,(T_2 = 52\mathrm{K}) \to \mathrm{FS}\,(T_3 = 20\mathrm{K}). \quad (2.1)$$

The intermediate CS phase represents a superposition of two LSW and SS phases with one and the same wave vector. In the high-temperature LSW phase, the neutron-diffraction pattern contains odd-order satellites up to 17th order,[21] whose intensity increases as the phase-transition point T_3, where the modulation of the z-components of the spins is replaced by a ferromagnetic state with a uniform spontaneous moment oriented along the z axis of the crystal, is approached. In addition, third- and fifth-order satellites, corresponding to components of spin vectors in the basal plane, are visible in the CS phase (temperature interval $T_2 > T > T_3$) (Fig. 6).

Higher-order satellites can also arise when a magnetic field is imposed on the modulated structures. Thus an SS structure, which transforms into a FAN structure in a field lying in the rotational plane of the spins, exists in MnP at low temperatures. This transition is accompanied by the appearance of higher-order satellites, whose intensity increases with the field.

c) Temperature-induced phase transitions. As the temperature is changed, phase transitions often appear between the modulated and the usual magnetic phases (see Tables I–III). The cases of transitions between IC and C phases due to the continuous approach of the wave vector $\mathbf{K}$ to the value $\mathbf{K}_0$, describing the commensurate phase, are of special interest. Two cases quite often arise here: when a modulated phase first appears as the temperature is decreased and then the commensurate phase appears (the transition IC→C) and vice versa (the transition C→IC). We present examples of phase transitions between IC and C phases, arising when the temperature is decreased:

HC → C:

$TbAu_2$, $DyAu_2$, $DyAg_2$ (D_{4h}^{17}):

$$\mathrm{TSW}, \quad [\mu\,\mu\,0] \to \left[\tfrac{1}{2}\ \tfrac{1}{2}\ 0\right], \quad (2.2)$$

Tb, Dy, Ho (D_{6h}^4):

$$\mathrm{SS} \to \mathrm{F}, \quad [0\,0\,\mu] \to 0, \quad (2.3)$$

Tm (D_{6h}^4):

$$\mathrm{LSW} \to \mathrm{F}, \quad [0\,0\,\mu] \to 0, \quad (2.4)$$

C → HC:

MnP (D_{2h}^{16}):

$$\mathrm{F} \to \mathrm{SS}, \quad 0 \to [0\,0\,\mu], \quad (2.5)$$

Cr_5S_6 (D_{3d}^2):

$$\mathrm{A} \to \mathrm{SS}, \quad \left[0\,0\,\tfrac{1}{2}\right] \to [0\,0\,\mu]. \quad (2.6)$$

We shall show below that the IC and C phases here are symmetrically related, just as the symmetry of the Lifshitz point and its neighborhood are related. There also exist other cases of phase transitions in which there is no symmetry relation between the IC and C phases and the phase transition between them (first-order) is due to the trivial equality of the free energy of the two phases at some temperature. We shall be most interested in the phase transitions IC⇄C, where the symmetry of the IC phase with the wave vector $\mathbf{K} = \mathbf{K}_0 + \mathbf{k}$ and of the C phase with the wave vector $\mathbf{K} = \mathbf{K}_0$ are related by the commensurability relations.

d) Field-induced phase transitions. In a magnetic field, the modulated structure can transform into a commensurate

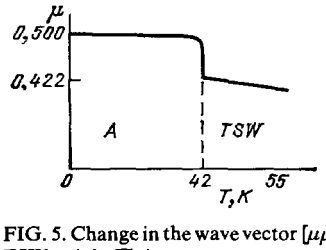

FIG. 5. Change in the wave vector $[\mu\mu 0]$ accompanying the phase transition TSW→A in TbA_2.

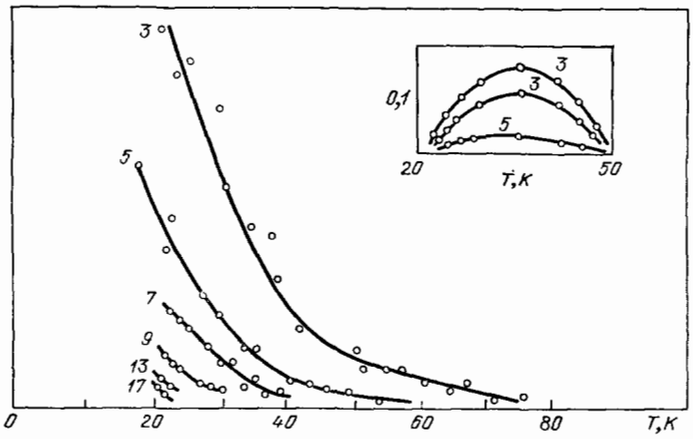

FIG. 6. Behavior of the intensity of the higher-order satellites in Er as a function of the temperature.

structure, which corresponds to a paramagnet in an external field (P structure with uniform magnetization along the field). This transition proceeds via the formation of an intermediate FAN structure with the magnetic moments oriented predominantly along the field. Such transitions have been studied in greatest detail in MnP and rare-earth metals. MnP has an orthorhombic structure. Three of its axes are usually chosen in accordance with the inequalities $a > b > c$ between the lattice constants. MnP undergoes a phase transition at $T_1 = 291$ K into a ferromagnetic structure with the spins oriented along the c axis. A second phase transition into the spiral SS phase occurs at $T_2 = 47$ K; here the wave vector is oriented along the a axis, while the spins rotate in the b, c plane. When a field is applied along the b axis, the phase diagram shown in Fig. 7 arises. The FAN phase appears in addition to the F and SS phases. The local magnetic moment in this phase oscillates in the b direction, always remaining in the b, c plane. The phase transitions F→SS and SS→FAN are first-order transition, and the triple point, where all three phases meet, is an ordinary triple point. The other triple point, where the F, FAN, and P phases meet, is a Lifshitz point. Its special properties consist of the fact that as it is approached the wave vector of the modulated phase (the FAN structure) continuously approaches zero. It now appears that MnP is the only magnetic system when a Lifshitz point is realized.

Neutron-diffraction studies have shown[22] that in a magnetic field, corresponding to the FAN structure, second-order satellites are observed together with the main magnetic satellites indicating the existence of the modulated phase and the wave vector depends on the magnitude of the magnetic field. For example, at $T = 77$ K, the wave vector increases linearly with the field for $H > 10$ kOe.

Another example is $MnAu_2$, which exhibits an SS structure with the wave vector lying along the tetragonal axis. When a field is applied in the basal plane, the intensity of the magnetic satellites practically does not change up to fields of ~ 10 kOe, but in a field of ~ 12 kOe a sharp drop in the intensity of the satellites, which is identified with the transition into the FAN structure, occurs. A sharp increase in the magnetization due to the rearrangement of the spiral magnetic structure into a fan structure is observed in the same range of fields (Fig. 8).

The isomorphic compounds of cerium CeSb and CeBe are unique examples of the complex behavior of the modulated structure accompanying a change in the temperature or the external field. In the paramagnetic phase, they have an fcc structure of the NaCl type. In CeSb, six different magnetic phases, which exist in a temperature range of the order of 1 degree, are observed in zero magnetic field in a narrow temperature interval (16K–8K). All phases are modulated with the wave vector $\mathbf{k} = (2\pi/a)(00k)$ oriented along the edge of a cube and with the spins aligned along the direction of the wave vector. One would thus think of the LSW structure, but the observation of harmonic satellites (of third-order) led in Refs. 48–51 to the proposition that a square spin-wave type structure, i.e., a structure with periodically arranged antiphase domains, is realized. The wave vector of each of the six phases assumes commensurate values, characterized by rational values of $k = 2/3$, 8/13, 4/7, 5/9, 6/11, and 1/2.[50] A

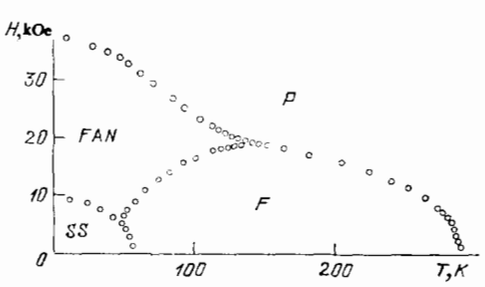

FIG. 7. Phase diagram for MnP in the (H, T) plane.

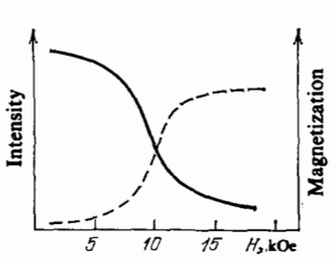

FIG. 8. Field dependence of the magnetization and intensity of the magnetic satellite in $MnAu_2$.

first-order phase transition is observed at the Neel point $T_N = 16$ K. A first-order phase transition into the antiferromagnetic structure of the IA type (fcc), which remains stable as the temperature is further decreased, is also observed at $T \approx T_N/2$. Temperature hysteresis is observed in transitions between intermediate phases with different k, which once again indicates first-order phase transitions. In a magnetic field, transitions between these phases are observed and new phases with values of $k = 2/5$ and $4/9$ appear.[51]

Thus a complicated cascade of transitions between commensurate, but modulated, phases occurs in CeSb. Such a complicated behavior of this material is a result of the strong exchange anisotropy: the exchange interaction within (001) planes is much stronger than between planes. Each separate plane is ordered ferromagnetically (a two-dimensional ferromagnet), but the weak coupling between planes can be easily destroyed by the temperature or a field. A model which takes into account the weak interplane interaction of nearest- and next-to-nearest-neighbors explains well the phase diagram in the (H, T) plane observed in CeSb.[54,55] The proposition in Refs. 48–51 that the magnetic structure of CeSb is formed by alternating ferromagnetic and paramagnetic planes is unlikely to be true, since the two-dimensional order in the planes must vanish at the same temperature. A more accurate neutron-diffraction analysis of this magnetic structure is therefore required.

In CeBi, only two magnetic phases with $k = 1/2$ and 1, describing the alternation of the magnetic moment in the planes $(+\ -\ +\ -)$ and $(+\ +\ -\ -)$, are observed in the absence of a field. In a magnetic field, phases with $k = 6/11$, $5/8$, and so on appear.[52,53] Some of these phases vanish when pressure is applied.[53]

Phase transitions in CeSb and CeBi accompanying a change in the temperature or the field proceed between phases characterized by commensurate values of the wave vector. The dependence of the vector $\mathbf{k}$ is thus represented by a discontinuous function of the temperature or of the field, a phenomenon which is called the "devil's staircase" (see the reviews Refs. 3 and 56). The reasons that the commensurate values of the wave vector are preferred energetically will be discussed below.

Another interesting example is chromium, in which modulated magnetic structures (of the spin-wave type) were first discovered.[5] It has now been firmly established that in Cr a TSW structure, which at $T_1 = 124$ K transforms into the LSW structure, arises below $T_N = 312$ K. This orientational phase transition TSW→LSW is accompanied by the appearance of a charge-density wave with vector $2k$ (k is the vector of the small modulation of the magnetic structure with $\mathbf{K}_0 = (2\pi/a)(0\ 0\ 1/2)$) in the LSW phase and the appearance of the third harmonic of the magnetic-moment density (see Ref. 57). A pronounced change in the magnetic structure occurs in a magnetic field.[58]

We shall now discuss the question of the magnitude of the modulation vector, i.e., the parameter μ, for the substances presented in Table I. The typical values $\mu \ll 1$ correspond to a change in the phase on two neighboring atoms, lying in the direction of the vector $\mathbf{k}$, by an amount of the order of radian. Anomalously small values of μ (i.e., very long periods of modulation of the magnetic structure) are observed in sprial structures in two isomorphic cubic compounds MnSi and FeGe. In MnSi the magnetic period is equal to 172 Å. When the manganese is replaced by cobalt, the period decreases; with a concentration of 4% Co it becomes equal to 106 Å. Even longer periods are observed in the alloys $Fe_x Co_{1-x} Si$[59] $(0.3 < x < 0.9)$. For $x = 0.3$ the pitch of the spiral reaches a value of 2300 Å. These alloys have the same crystalline structure as the compounds MnSi and FeGe. Their space group T^4 does not contain a center of inversion, which permits the existence of strongly anisotropic inhomogeneous interactions of relativistic origin in the crystal. As we shall see below, they lead a modulation of the magnetic structure, whose wave vector $\mathbf{k}$ is proportional to the magnitude of this interaction and is therefore small.

In the overwhelming majority of magnetically ordered crystals, the symmetry does not permit such interactions in the crystal and the competition between the positive and negative exchange interactions is responsible for the modulation. In this situation, there is, in general, no reason for the very small value of the wave vector of the modulation, which must be determined by the ratio of the exchange integrals. Indeed, for a chain of classical spins with an exchange integral $J_1 > 0$ for nearest neighbors and $J_2 < 0$ for the next-to-nearest neighbors, the angle φ between the spins of two neighboring atoms is determined by the obvious relation

$$\cos\varphi = \frac{J_1}{4|J_2|}.$$

For the formation of the modulated phase it is sufficient that $J_1/4|J_2| < 1$. Since J_1 and $|J_2|$ are of the same order of magnitude, the angle φ can be arbitrary, i.e., the wave vector of the modulation is not necessarily small.

3. THE GINZBURG-LANDAU FUNCTIONAL

All the above-described phenomena, namely, the change in the wave vector with the temperature or field, the appearance of higher-order satellites, and the transitions between the C and IC phases, are closely interrelated. This can be understood based on a study of the free-energy functional for an inhomogeneous distribution of the order parameter (OP).

There are two approaches to the phenomenological theory of modulated phases with a wave vector $\mathbf{K}$, terminating at the unsymmetrical (non-Lifshitz) points of the Brillouin zone. First of all, an invariant expansion can be written down for the nonequilibrium function Φ in powers of the OP, starting from the intrinsic symmetry of the vector $\mathbf{K} = \mathbf{K}_0 + \mathbf{k}$. The number of components n of the OP is determined by the number of rays in the star of the vector $\mathbf{K}$ and by the dimensionality of the irreducible representation, characterizing the given modulated structure. This approach, which takes into account the complete set of components of the OP, is necessary for studying the fluctuation region in the paramagnetic phase of the crystal,[24,25] for example, in determining the critical indices of the phase transition.

In the alternative method, Φ is written down starting from the symmetry of the vector $\mathbf{K}_0$—of the Lifshitz point. For it, the dimensionality of the corresponding OP of the symmetry group of the initial phase is less than n. The inclusion in Φ of inhomogeneous terms, depending on the spatial derivatives of the OP, leads to inhomogeneous solutions of the equations of minimization for the OP. They can be classified according to the star of the wave vector $\mathbf{K}_0 + \mathbf{k}$, which is what makes both approaches equivalent. The second approach is possible because the symmetry of the Lifshitz point also determines the symmetry of its entire neighborhood. Since the modulation vector $\mathbf{k}$ is usually much smaller than the reciprocal lattice vector, we can use the second method, i.e., we start from the functional for the Lifshitz point.

The convenience of this description is linked to the fact that the potential at the Lifshitz point (more symmetrical than the points in its neighborhood) is simpler and can be obtained more easily. Next, we must choose a solution of the equation of minimization of Φ that describes the modulated phase, guided by the following considerations. Structures modulated in one direction arise in crystals, and in searching for the corresponding phase only invariants with derivatives with respect to one spatial coordinate need be included in the functional.

In itself, this fact follows from neutron-diffraction analysis. The modulated structure is indicated by the appearance of satellites lying near the sites of the reciprocal lattice (or symmetrical points of the zone). The distance from the satellite to the nearest site determines the modulation vector $\mathbf{k}$. If $\mathbf{k}$ lies along the principal axis of the crystal, then there exists a pair of equidistant satellites, corresponding to rays of the star $\mathbf{k}$ and $-\mathbf{k}$ (Fig. 2a). If $\mathbf{k}$ lies, for example, along the edge of a cube, then a hexad of satellites, corresponding to a six-ray star must appear, and so on (Fig. 2b). Each pair of satellites in Fig. 2b corresponds to modulation in one of the directions x, y, or z. In neutron-diffraction studies the observation of a hexad of satellites is taken to mean that there are three types of domains with modulations in three independent directions. Within a single domain, the magnetic structure is described only by two rays $\mathbf{k}$ and $-\mathbf{k}$, corresponding to a spatial inhomogeneity in one direction. Possible exceptions are Nd and $CeAl_2$, where a multi-$\mathbf{k}$-structure with modulations in several directions simultaneously has been proposed.[4]

Another advantage of the method of description with the help of the Lifshitz point appears in the study of the modulated phases in external fields, when the structure in the external field is not known, but we want to find it. If the external field does not transfer the structure into a different Lifshitz point (in other words if it is not too large), then the wanted phase can be sought amongst the solutions of the equations of minimization of the functional taking into account the interaction with this field.

We shall examine a typical form of the potential Φ for a two-component OP, which, as we shall see below, describes many real situations in crystals:

$$\Phi = \int dz\, [r(\eta\xi) + u(\eta\xi)^2 + w(\eta^n + \xi^n) + V_{\text{inhom}}(z)]. \quad (3.1)$$

We shall assume that this functional corresponds to the symmetry of the vector $\mathbf{K}_0$. Here, η and ξ are complex conjugates of one another; the parameters r and u satisfy the standard contitions of Landau's theory: $r \sim (T - T_c), u > 0$; and the sign of w in the third term, describing the nth order anisotropy, can be arbitrary. The last term in Φ, containing the spatial derivatives of the OP, can have two forms, depending on the symmetry of the vector $\mathbf{K}_0$:

$$V_{\text{inhom}}(z) = \begin{cases} i\sigma\left(\eta\frac{d\xi}{dz} - \xi\frac{d\eta}{dz}\right) + \gamma\frac{d\eta}{dz}\frac{d\xi}{dz}, & \gamma > 0 \quad \text{(D)}, \\ \gamma\frac{d\eta}{dz}\frac{d\xi}{dz} + \alpha\frac{d^2\eta}{dz^2}\frac{d^2\xi}{dz^2}, & \alpha > 0 \quad \text{(M)}, \end{cases} \quad (3.2)$$

i.e., either it contains a Lifshitz invariant which is linear with respect to the derivatives or it does not. In the case D (Dzyaloshinskiĭ[26]), the appearance of the inhomogeneity is energetically favorable for any sign of σ, while in the case (Michelson[27]), the appearance of the inhomogeneity is energetically favorable only for $\gamma < 0$.

The rest of the analysis of the magnetic structures and of phase transitions will be based on the phenomenological Landau theory. It is, however, appropriate to describe here, even briefly, the microscopic meaning of the different terms in the Ginzburg-Landau functional for a two-component OP—expressions (3.1) and (3.2).

Invariants of the form

$$\eta\frac{d\xi}{dz} - \xi\frac{d\eta}{dz}$$

which are linear in the derivatives can appear from expressions of the type $\mathbf{M}$ curl $\mathbf{M}$, describing the relativistic Dzyaloshinskiĭ—Mori interaction.[60] For a cubic crystal without a center of inversion, the expression $\mathbf{M}$ curl $\mathbf{M}$ is an invariant. For example, such an invariant exists in MnSi and FeGe crystals with the space group T^4; and, on the other hand, an SS structure with a very long magnetic period, indicating the weak (relativistic) nature of the inhomogeneous magnetic interactions, is observed in these crystals. The inhomogeneous terms in the functional (3.1) with even derivatives of the OP (case M) describe the inhomogeneous parts of the exchange energy and correspond to invariants of the form $(\partial\mathbf{M}/\partial x_\alpha)\,\partial\mathbf{M}/\partial x_\alpha$ and $(\partial^2\mathbf{M}/\partial^2 x_\alpha)\,\partial^2\mathbf{M}/\partial^2 x_\alpha$, formed by the components of the local magnetic-moment vector. The transformation from the variables $\mathbf{M}$ to the components of the OP is implemented with the help of the symmetry of the system being described, and specific examples will be given below in Secs. 6 and 7.

The advantage of the phenomenological description with the help of the OP lies in the fact that it is possible to describe in a unified manner phase transitions in crystals with different structural complexity and thereby to clarify the general mechanisms of the transitions. A disadvantage is that all parameters in the Ginzburg-Landau functional are assumed to be unknown. In reality, in deriving these functionals from microscopic Hamiltonians we would see that some of these parameters are interrelated and therefore, in particular, the problem of the stability of the equilibrium phases, obtained by minimizing the functional, would be solved more definitely. The complete joining of the pheno-

menological and microscopic approaches in the theory of phase transitions thus consists of obtaining a microscopic derivation of the Ginzburg-Landau functionals.

We note that functionals of the type (3.1) are introduced in order to describe a single phase transition from the paramagnetic phase, since an OP which transforms according to a single irreducible representation is included. If we are dealing with a cascade of transitions, then all OP describing each of the phases must be examined and a functional for interacting order parameters must therefore be introduced. Each of the phases has its own region of stability in the space of the parameters of the functional (coefficients with independent invariants) and temperature. For example, the orientational phase transition TSW→LSW in Cr must be described by two interacting OP: one of them (two-component) describes the TSW phase and the other (single-component) describes the LSW phase. The sequence of phase transitions, for example, accompanying a change in temperature is detemined by the parameters of the Ginzburg-Landau functional (their sign and magnitude). It is in this spirit that the magnetic phase transitions in Cr are explained.[57]

Near a phase transition from the paramagnetic phase into the magnetically ordered phase, the terms in the functional (3.1) $\sim u$ and $\sim w$, containing higher-order powers of the OP, can be dropped. It is then easy to verify that the spatial distribution of the OR is described by a single harmonic:

$$\eta(z) = A_1 e^{ik_0 z}, \quad A_1 = \sqrt{-\frac{r}{2u}} \sim \sqrt{T_c - T}, \tag{3.3}$$

and, in addition, the wave vector of the modulation $\mathbf{k} = [00k_0]$ is expressed in terms of the parameters describing the term $V_{\text{inhom}}(z)$[26,27]:

$$k_0 = \begin{cases} \frac{|\sigma|}{\gamma} & \text{(D)}, \\ \sqrt{\frac{-\gamma}{2\alpha}} & \text{(M)}. \end{cases} \tag{3.4}$$

As the temperature is decreased, the amplitude of the OP A_1 increases, and the fourth- and nth order terms in the functional (3.1) must generate multiple harmonics, which are manifested experimentally as higher-order satellites. The spatial distribution of the magnetic moment $\mathbf{M}(z)$ is expressed in terms of the OP $\eta(z)$ and $\xi(z)$ by the general relation

$$\mathbf{M}(z) = \mathbf{m}\eta(z)\, e^{ik_0 z} + \mathbf{m}^*\eta^*(z)\, e^{-ik_0 z}, \tag{3.5}$$

where $\mathbf{m}$ is a constant vector. If $\mathbf{m}$ is complex, then expression (3.5) determines a sprial structure; if $\mathbf{m}$ is real, then (3.5) determines a TSW structure. The pattern of the spatial distribution of the OP $\eta(z)$ will be different in the cases (D) and (M). We shall study it for systems which admit Lifshitz invariants in the functional Φ.

4. SYSTEMS ADMITTING LINEAR LIFSHITZ INVARIANTS

Phase transitions in systems with linear invariants were first studied by Dzyaloshinskiĭ[26] in the approximation of a constant modulus of the OP:

$$\rho = \text{const}. \tag{4.1}$$

The modulus ρ and the phase φ are defined by the relations $\eta = \rho e^{i\varphi}$ and $\xi = \rho e^{-i\varphi}$.

In this approximation the functional Φ for the case (D) depends only on the single quantity $\varphi(z)$:

$$\Phi = \int dz \left[\gamma\rho^2 \left(\frac{d\varphi}{dz}\right)^2 + 2\sigma\rho^2 \frac{d\varphi}{dz} + 2w\rho^n \cos n\varphi\right]. \tag{4.2}$$

Variation of Φ leads to the following equation for the phase:

$$\frac{d^2(n\varphi)}{dz^2} + v \sin(n\varphi) = 0, \tag{4.3}$$

where n is the effective anisotropy parameter:

$$v = n^2 \frac{w}{\gamma} \rho^{n-2}. \tag{4.4}$$

In the absence of anisotroy, Eq. (4.3) has the solution $\varphi = kz$, which describes a one-harmonic incommensurate structure, for example, a simple spiral. On the other hand, Eq. (4.3) also has a uniform solution $\varphi = 0$, corresponding to a commensurate structure. For finite v, Eq. (4.3) must describe some inhomogeneous distribution of the phase of the OP, given by its exact solution, expressed in terms of the elliptic function of the amplitude:

$$\varphi = \frac{2}{n} \operatorname{am}(qz, \varkappa), \tag{4.5}$$

where $q = \sqrt{v}/\varkappa$, and $\varkappa$ is the modulus of the elliptic functions. The parameter $\varkappa$ corresponds to the constant of integration of Eq. (4.3) and must be found from the energy minimum of the system. (The second constant of integration, the initial coordinate z_0, is set equal to zero.)

The energy of the state in which the distribution of the OP was described by Eq. (4.5), is expressed in terms of the complete elliptic integrals K and E of the first and second kind[26]:

$$\frac{\Phi}{\rho^2} = -2|\sigma| \frac{\pi\sqrt{v}}{n\varkappa K} + 2\gamma \frac{v}{n^2} \left(\frac{\varkappa^2 - 2}{\varkappa^2} + \frac{4}{\varkappa^2} \frac{E}{K}\right). \tag{4.6}$$

Minimization of this equation with respect to $\varkappa$ leads to an equation for $\varkappa$:

$$\frac{E}{\varkappa} = \sqrt{\frac{v_c}{v}}, \quad v_c = \frac{n^2\pi^2\sigma^2}{16\gamma^2}. \tag{4.7}$$

The modulus $\varkappa$ varies over the range $0 < \varkappa < 1$ as the effective anisotropy parameter varies, correspondingly, from 0 to v_c. For this variation of $\varkappa$, the form of the amplitude function changes drastically. As can be seen from Fig. 9, a periodic

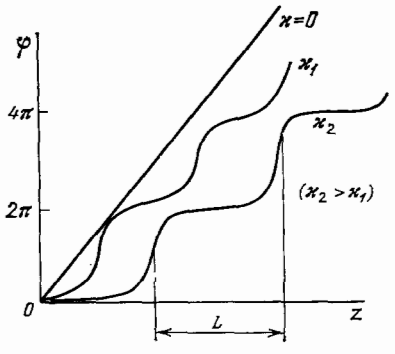

FIG. 9. Graph of the amplitude of the elliptic function as a function of the modulus $\varkappa$.

structure with some periodic L, which evolves as the parameter v varies, arises. As v is increased, a section appears within the period l where the phase is almost constant, but the phase changes markedly at the ends of the period, where a change in phase by $2\pi/n$ occurs. In the limit $v \to v_c$, the relative fraction of the section of constant phase increases. Under these conditions the system can be represented as a periodic structure of domains of the commensurate phase (with a constant value of φ equal to a multiple of $2\pi/n$) separated by domain walls—solitons. The period of the function (4.5) is

$$L = \frac{4\varkappa K}{\sqrt{v}}. \tag{4.8}$$

The soliton pattern described above can be easily seen from Eq. (4.5) by making use of the asymptotic expansion of the elliptic integrals[28]:

$\varkappa \to 0$:

$$K = \frac{\pi}{2}\left(1 + \frac{\varkappa^2}{4} + \ldots\right), \quad E = \frac{\pi}{2}\left(1 - \frac{\varkappa^2}{4} + \ldots\right), \tag{4.9}$$

$\varkappa \to 1$ $(\varkappa' \equiv \sqrt{1-\varkappa^2} \to 0)$:

$$K = \ln\frac{4}{\varkappa'} + \ldots, \quad E = 1 + \frac{1}{2}\varkappa'^2 \ln\frac{4}{\varkappa'} + \ldots. \tag{4.10}$$

It follows from (4.8) and (4.10) that the period of the soliton lattice diverges logarithmically as $v \to v_c$. Since the wave vector of the modulation $k \sim 1/L$, it is clear that as $v \to v_c$, $k \to 0$, i.e., in this limit the wave vector of the incommensurate phase approaches its commensurate value K_0. The commensurate phase remains stable as the parameter v changes further, i.e., as the temperature is decreased. Thus Dzyaloshinskiĭ's theory describes the phenomenon of locking of the wave vector in the case of an IC→C type phase transition.

We shall illustrate the evolution, described by the solution (4.5), of the spatial distribution of the OP for the example of the sprial structure SS. Let the wave vector of the spiral be oriented along the principal axis of the crystal (z axis) and let the magnetic moment lie in the basal x, y plane. The magnetic anisotropy in this plane is described by the invariant $(M_x + iM_y)^n + (M_x - iM_y)^n$, which in terms of the OP was written in the form $\eta^n + \xi^n$ (see expression (3.1). The nth order anisotropy distinguishes n equivalent directions in the plane along which the atomic magnetic moments try to align themselves. If there is no anisotropy, then the magnetic moments turn smoothly from layer to layer along the z axis. If the anisotropy is infinitely large, then they cling to one of the n distinguished directions. According to Fig. 10, as the temperature is decreased, the parameter v increases with $\varkappa$—the modulus of the OP. At $v = v_c$ the magnetic moments of the entire packet of planes of size L are oriented parallel to one another in the direction of one of the anisotropy axes; as we move along the z axis, they rapidly rotate toward the neighboring axis and remain in this orientation over the length L; then they turn toward the next axis; and so on. The transition from one axis to a neighboring one, accompanied by a change in phase by $2\pi/n$, corresponds to the domain wall (soliton) (Fig. 10).

The predicted structure of the incommensurate phase can be checked experimentally by the neutron-scattering method. To analyze the neutron-diffraction pattern, the OP

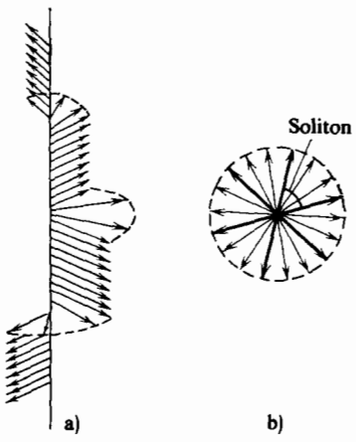

FIG. 10. Spiral structure in the presence of anisotropy in the basal plane. a) Side view; b) view from above.

must be expanded in a Fourier series. The structure of the series can be understood from the well-known expansion of the amplitude function.[28] For the phase (4.5), we have

$$\varphi(z) = \frac{\pi}{nK} qz + \sum_{p=1}^{\infty} \frac{2}{n \operatorname{ch}(\pi K' p/K)} \sin\left(p \frac{\pi}{K} qz\right), \tag{4.11}$$

where $K(\varkappa)$ and $K' = K(\varkappa')$ are the complete elliptic integrals of the first kind.

From the expression of the OP in terms of the phase φ, we see that the quantity

$$k = \frac{\pi q}{nK} \tag{4.12}$$

represents the wave vector of the structure. The sum over p in expression (4.11) leads to multiple harmonics in the distribution of the OP; in addition, the Fourier series for $\eta(z)$ contains harmonics of the following orders:

$$\pm p = n \pm 1, \quad 2n \pm 1, \quad 3n \pm 1, \ldots. \tag{4.13}$$

The amplitude of the harmonics decreases rapidly with p, since it is determined by the factor $\operatorname{ch}^{-1}(\pi K' p/K)$. The structure of the harmonic series for the OP is shown in Fig. 11. The amplitude of the harmonics and the wave vector depend on the temperature via the parameter $\varkappa$. For $\varkappa = 0$, as follows from the asymptotic series (4.9) and (4.10), only the fundamental harmonics $e^{\pm ikz}$ remain in the series for $\eta(z)$. As $\varkappa$ is increased, higher-order harmonics, whose amplitude increases, while the distance between them decreases, appear. As $\varkappa \to 1$ (which corresponds to $v \to v_c$), the harmonics coalesce, forming a quasicontinuous spectrum.

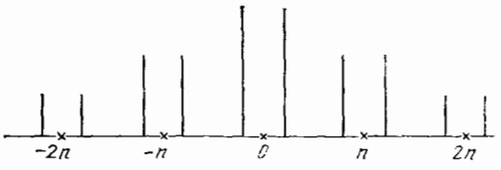

FIG. 11. Fourier series for the order parameter, described by the Dzyaloshinskiĭ solution (schematically).

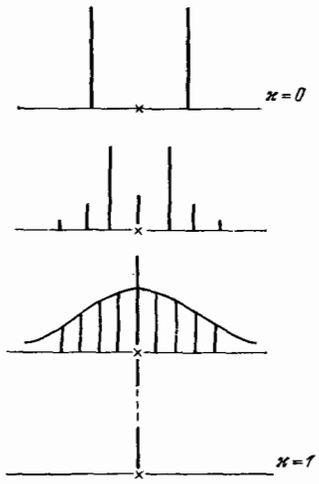

FIG. 12. Evolution of the harmonic series for the distribution of the order parameter in the presence of a first-order anisotropy ($n = 1$ corresponds to the external magnetic field).

The evolution of the harmonic series for $\eta(z)$ is shown in Fig. 12 for the case $n = 1$. The first-order anisotropy corresponds to the external field. The appearance of the central harmonic, which increases sharply with the field and draws into itself the entire intensity of the distribution at $\varkappa = 1$, is characteristic for this case. Figure 12 thus describes a smooth transition from the incommensurate phase with two fundamental harmonics in the distribution of the OP ($p = \pm 1$) to the commensurate phase with the central harmonic ($p = 0$). This is the phase with uniform magnetization.

The neutron-diffraction pattern can be derived from the general expression for the elastic magnetic scattering cross sections[4]:

$$\frac{d\sigma}{d\Omega} \sim \sum_{\alpha\beta\gamma\gamma'} K_{\gamma\gamma'} (\delta_{\alpha\gamma} - e_\alpha e_\gamma) \times (\delta_{\beta\gamma'} - e_\beta e_{\gamma'}) F_\alpha^* (\mathbf{Q}) F_\beta (\mathbf{Q}), \quad (4.14)$$

where $\mathbf{Q}$ is the scattering vector and $\mathbf{e}$ is the unit scattering vector; the quantity $K_{\gamma\gamma'}$ represents the product $\sigma_\gamma \sigma_{\gamma'}$, where σ_γ is a Pauli matrix, averaged over the spins of the neutrons in the incident beam; and $\mathbf{F}(\mathbf{Q})$ is the Fourier component of the magnetic-moment density in the crystal.

Consider the scattering by an SS structure with the wave vector k lying along the z axis and the spins lying in the x, y plane. This structure is described by the relations

$$M_x = M_0 \cos\varphi, \quad M_y = M_0 \sin\varphi, \quad M_z = 0. \quad (4.15)$$

In the absence of an external field or anisotropy, the phase $\varphi = kz$, and the scattering of polarized neutrons is described by the expression[29]

$$\frac{d\sigma}{d\Omega} \sim \sum_{\mathbf{b}} \sum_{+,-} [1 + (\mathbf{em})^2 \pm 2(\mathbf{em})(\mathbf{ep}_0)] \delta(\mathbf{Q} - \mathbf{b} \pm \mathbf{k}), \quad (4.16)$$

where $\mathbf{b}$ is an arbitrary reciprocal lattice vector of the crystal and the delta function determines the position of the two Bragg magnetic peaks near each site of the reciprocal lattice with $\mathbf{Q} = \mathbf{b} \mp \mathbf{k}$. Their intensity is determined by the mutual

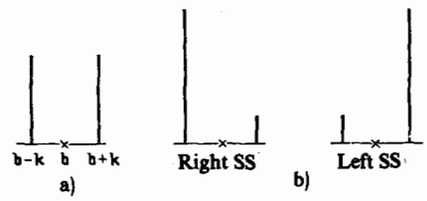

FIG. 13. Magnetic satellites for a simple spiral in the presence of scattering of unpolarized (a) and polarized (b) neutrons.

orientation of the vector $\mathbf{e}$, the polarization of the beam $\mathbf{p}_0$, and the vector of the spiral $\mathbf{m}$. The latter represents a unit pseudovector, perpendicular to the rotational plane of the spins. It is evident from (4.16) that for unpolarized neutrons the intensities of both magnetic satellites are the same, whereas for polarized neutrons they depend on the orientation of $\mathbf{p}_0$, $\mathbf{e}$, and $\mathbf{m}$. It is easy to choose an orientation of vectors such that one of the satellites will be completely suppressed, while the intensity of the second satellite will be doubled (for a homogeneous sample, representing a right- or left-handed spiral) (Fig. 13).

We now take into account the nth order anisotropy in the basal plane. The harmonics in the distribution of the OP lead to the appearance of higher-order satellites in the diffraction pattern. The scattering cross section, calculated form Eq. (4.14) for $n = 1$, is given by the following expression[30]:

$$\frac{d\sigma}{d\Omega} \sim \sum_{\mathbf{b}} J_0^{x^2}(\varkappa)(1 - e_x^2)\delta(\mathbf{Q} - \mathbf{b}) + \sum_{\mathbf{b}} \sum_{+,-} \sum_{p=1}^{\infty} [J_p^{x^2}(\varkappa)(1 - e_x^2) + J_p^{y^2}(\varkappa)(1 - e_y^2) \pm 2 J_p^x(\varkappa) J_p^y(\varkappa)(\mathbf{p}_0 \mathbf{e}) e_z)] \delta(\mathbf{Q} - \mathbf{b} \pm p\mathbf{k}). \quad (4.17)$$

It describes the scattering cross section in a magnetic field applied in the basal plane along the $-x$ axis. The amplitudes $J_p^\alpha(\varkappa)$ depend on the modulus of the elliptic function $\varkappa$:

$$J_0^x(\varkappa) = 1 + \frac{2(E-K)}{\varkappa^2 K}, \quad J_p^x(\varkappa) = \frac{\pi^2}{\varkappa^2 K^2} \frac{p}{\operatorname{sh}(p\pi K'/K)}, \quad J_p^y(\varkappa) = \frac{\pi^2}{\varkappa^2 K^2} \frac{p}{\operatorname{ch}(p\pi K'/K)}, \quad (4.18)$$

while the quantity $\varkappa$ is expressed in terms of the field h (more precisely $h = H/M_0$) by means of the equation

$$\frac{E}{\varkappa} = \sqrt{\frac{h_c}{h}}, \quad h_c = \frac{\pi^2 \sigma^2}{8\gamma} \quad (4.19)$$

(this is actually Eq. (4.7) rewritten for $n = 1$).

In weak field $\varkappa \ll 1$ and with the help of the asymptotic expansions (4.9) we obtain

$$J_1^x(\varkappa) = \frac{1}{2} - \frac{3}{2}\left(\frac{\varkappa}{4}\right)^4 + \ldots, \quad J_1^y(\varkappa) = \frac{1}{2} - \frac{5}{2}\left(\frac{\varkappa}{4}\right)^4 + \ldots,$$

$$J_0^x(\varkappa) = -\frac{1}{8}\varkappa^2 + \ldots,$$

$$J_p^x(\varkappa) = J_p^y(\varkappa) = \frac{p}{2}\left(\frac{\varkappa}{4}\right)^{2p-2} + \ldots \quad (p > 2);$$

where $\varkappa^2 = 2\gamma/\sigma^2 h$. It is evident from here that the intensity of the central peak is $\sim h^2$ (the principal satellites decrease in

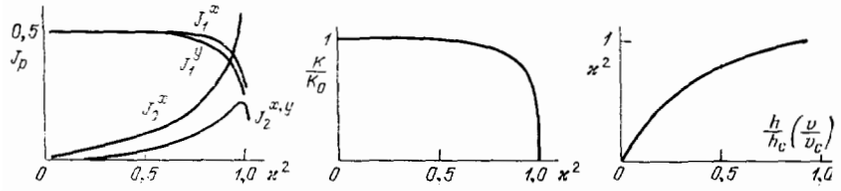

FIG. 14. Dependence of the amplitudes $J_p(\varkappa)$ of the pth order satellites and of the wave vector of the spiral as a function of the magnetic field applied in the plane of rotation of the spins.

the same degree), while the intensities of the pth order satellites are $\sim h^{2p-2}$.

In the other limiting case, $\varkappa \to 1 (h \to h_c)$, the asymptotic expansion (4.10) shows that the wave vector k approaches zero logarithmically, and all reflections approach the central peak, whose intensity is $\sim [J_0^x(\varkappa)]^2 \to 1$. In expression (4.17) the summation over p can be replaced by integration, as a result of which the cross section is described by the equation

$$\frac{d\sigma}{d\Omega} \sim \sum_b \left(1 - \frac{4}{\ln \frac{4}{\varkappa'}}\right)(1-e_x^2)\,\delta(\mathbf{Q}-\mathbf{b}) + \sum_b \frac{8}{\pi^2 \Delta \ln \frac{4}{\varkappa'}} \left(\frac{Q_z - b_z}{\Delta}\right)^2 \times \left[\frac{1-e_x^2}{\mathrm{sh}^2 \frac{Q_z-b_z}{\Delta}} + \frac{1-e_y^2}{\mathrm{ch}^2 \frac{Q_z-b_z}{\Delta}} - \frac{2e_z(\mathbf{p}_0\mathbf{e})}{\mathrm{sh}\frac{Q_z-b_z}{\Delta}\cdot \mathrm{ch}\frac{Q_z-b_z}{\Delta}}\right] \times \delta(Q_x - b_x)\,\delta(Q_y - b_y), \quad (4.20)$$

where $\Delta = (2/\pi)\sqrt{h/2\gamma}$. We can see that against the background of the diffuse peak of width Δ (along the z axis) there arises an intense central component, into which all scattering from the diffuse peak at $h = h_c$ is transferred. At this point a phase transition from the incommensurate into the commensurate structure occurs. The central peak arises due to the appearance of magnetization in an external field; in addition, its magnitude is given by the expression

$$M_x = M_0 \int dz \cos\varphi = M_0 J_0^x(\varkappa).$$

The dependence of the scattering amplitudes $J_p^\alpha(\varkappa)$ for arbitrary values of $\varkappa$, calculated from Eqs. (4.18) and (4.19), is shown in Fig. 14.

The natural crystalline anisotropy in the basal plane must give a qualitatively analogous scattering pattern, taking into account, of course, the thinning out of the higher-order satellites (see (4.13)). The main difference lies in the absence of the central peak, since the corresponding scattering is extinguished by domains of the commensurate phase with a different orientation of the anisotropy axis. (In the case of a magnetic field there is only one such axis!) Exact equations for the cross section can be obtained only for a second-order anisotropy.

A change in the field or the temperature essentially gives the same soliton picture of the phase transition and the same diffraction pattern. What happens if the crystalline anisotropy is also taken into account when a field is applied? In the approximation $\rho = \text{const}$ this leads to the following equation for the phase of the OP:

$$\frac{d^2\varphi}{dz^2} + v_1 \sin\varphi + v_n \sin(\varphi n) = 0, \quad (4.21)$$

where

$$v_1 = \frac{H}{2\gamma\rho}, \qquad v_n = \frac{nw\rho^{n-2}}{\gamma}.$$

It has exact solutions which can be expressed in terms of elliptic functions only for $n = 2$.[31,30] Here, two uniform solutions corresponding to the commensurate phases are possible:

$$1)\ \cos\varphi = -1, \quad 2)\cos\varphi = -\frac{H}{8w\rho}. \quad (4.22)$$

One solution corresponds to the ferromagnetic state, when the field is applied along the easy axis, the second corresponds to the spin-flop phase, when the field is applied along the difficult axis. In accordance with this, two nonuniform solutions arise: 1s with one type of soliton and 2s with two types of solitons.

Figure 15 clarifies the mutual relation of the phases. In the commensurate phase 1 all magnetic moments are oriented along the field. In the phase 1s they rotate around the z axis, but are most often located near the shaded sector. In phase 2, there are two energetically equivalent orientations of the magnetic moments (two domains). In phase 2s, they also rotate around the z axis, but are most often located near each of the shaded sectors. Thus there are two domain walls (two solitons) with a change in the phase φ of less than π and greater than π.

The phase diagram in the anisotropy-field plane is shown in Fig. 16. It represents a typical section of the volume phase diagram at a fixed temperature (not too close to T_c, where the formally obtained solutions are unstable). The phase transitions 1s→1 and 2s→2 from the incommensurate

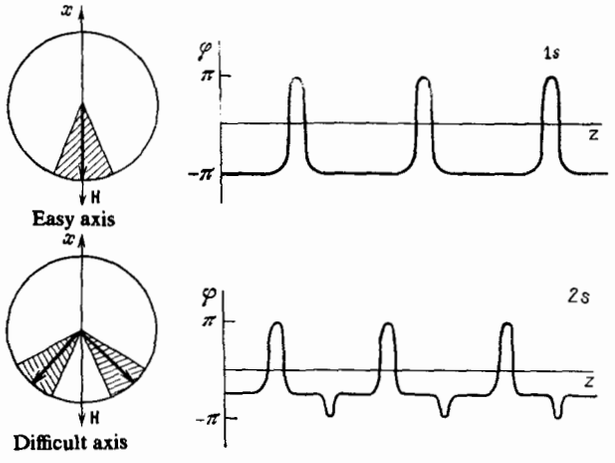

FIG. 15. Soliton picture of the incommensurate phase in the presence of a second-order anisotropy and an external magnetic field.

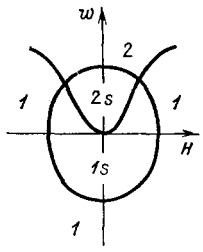

FIG. 16. Phase diagram in the presence of second-order anisotropy and an external magnetic field.

phase into the commensurate phase are first-order transitions with jumps in the OP. On the line separating the 2s and 1s phases, the states continuously transform into one another. It is suggested in Ref. 31 that this boundary is not the phase-transition line at all. On this line two systems of satellites (even and odd orders) of the 2s phase transform into a single system of satellites of the 1s phase. It would be possible to determine the boundary between the incommensurate phases from this change in the diffraction pattern. Near the boundaries of the transition into the commensurate 1s or 2s phase, there arises a pattern of converging satellites with a marked increase in the central peak.

In the case of an anisotropy of arbitrary order, the neutron diffraction pattern can be obtained from perturbation theory.[30] For low fields, it can be represented in a way such that each anisotropy-produced satellite generates its own field-produced supersatellites; thus a comb of satellites without omissions arises.

5. SYSTEMS WHICH DO NOT ADMIT LIFSHITZ INVARIANTS

The overwhelming majority of modulated magnetic structures in crystals are obtained as a result of the modulation of the initial ferro- or antiferromagnetic structure with wave vector $\mathbf{K}_0$, whose symmetry does not admit linear invariants (case M). For one- and two-component OP, it is necessary to work with the functionals

$$\Phi = \int dz \left[r\eta^2 + u\eta^4 + \gamma \left(\frac{d\eta}{dz}\right)^2 + \alpha \left(\frac{d^2\eta}{dz^2}\right)^2 \right], \quad (5.1)$$

$$\Phi = \int dz \left[r(\eta\xi) + u(\eta\xi)^2 + w(\eta^n + \xi^n) + \gamma \frac{d\eta}{dz}\frac{d\xi}{dz} + \alpha \frac{d^2\eta}{dz^2}\frac{d^2\xi}{dz^2} \right], \quad (5.2)$$

which we shall call 1M and 2M, respectively.

In expression (5.2) the term $w(\eta^n + \xi^n)$ describes the usual crystalline anisotropy, corresponding to the vector $\mathbf{K}_0$. For example, with $\mathbf{K}_0 = 0n = 4$ for a tetragonal crystal and $n = 6$ for a hexagonal crystal. In what follows we shall not examine any effects of commensurability based on this functional.

We shall first study the functional 1M for a single-component OP, describing, for example, the LSW phases. The spatial distribution of the OP satisfies a nonlinear differential equation

$$\hat{L}\eta + 2u\eta^3 = 0, \quad (5.3)$$

where $\hat{L}$ is the fourth-order differential operator:

$$\hat{L} = \alpha \frac{d^4}{dz^4} - \gamma \frac{d^2}{dz^2} + r. \quad (5.4)$$

It is hardly possible to find the exact solutions of this equation, so that we shall study the asymptotic behavior of the solutions near a phase transition. Near T_c, where the nonlinear term $\sim u\eta^3$ is small, the zeroth-order approximation with respect to the parameter u gives the solution $\eta_0 \sim \cos kz$. The nonlinear term $\sim \eta^3$ generates the odd harmonics, so that the solution of Eq. (5.3) must be sought in the form of a series

$$\eta = A_1 \cos kz + A_3 \cos 3kz + A_5 \cos 5kz + \ldots, \quad (5.5)$$

where the amplitudes A_p and the wave vector k must be determined from the minimum of the energy Φ_{IC}. The expression for the energy is obtained after substituting (5.5) into the functional (5.1) and integrating. Up to the first three harmonics we have[32]

$$\Phi_{IC} = \frac{1}{2}[L(k)A_1^2 + L(3k)A_3^2 + L(5k)A_5^2] + \frac{3}{8}u(A_1^4 + A_3^4 + A_5^4) + \frac{3}{2}u(A_1^2A_3^2 + A_1^2A_5^2 + A_3^2A_5^2) + \frac{1}{2}uA_1^2A_3^2 + \frac{3}{2}u(A_1^2A_3A_5 + A_1A_3^2A_5);$$

where $L(k)$ is an eigenvalue of the operator $\hat{L}$:

$$L(k) = \alpha k^4 + \gamma k^2 + r. \quad (5.6)$$

Minimization with respect to A_p permits expressing the amplitudes of all multiple harmonics in terms of the fundamental harmonic:

$$A_3 = -\frac{u}{2L(3k)}A_1^3, \quad A_5 = \frac{3u^2}{4L(3k)L(5k)}A_1^5, \ldots \quad (5.7)$$

and in the lowest approximation it is given by the relation

$$A_1 = \sqrt{-\frac{r}{2u}} \sim \sqrt{T_c - T}. \quad (5.8)$$

The wave vector is determined from the equation $\partial\Phi_{IC}/\partial k = 0$, i.e.,

$$L'(k)A_1^2 + 3L'(3k)A_3^2 + 5L'(5k)A_5^2 + \ldots = 0, \quad (5.9)$$

where the prime indicates differentiation with respect to the argument. Retaining the contribution of the first even harmonic only, we obtain from here

$$k^2 = k_0^2\left(1 - 24\frac{A_3^2}{A_1^2}\right), \quad (5.10)$$

where $k_0^2 = -\gamma/2\alpha$. Thus the appearance of multiple harmonics leads to a temperature dependence of the wave vector, determined by the factor $A_3^2/A_1^2 \sim A_1^2 \sim (T_c - T)$. The numerical coefficient here is small, so that the order of magnitude of the change in the quantity $\Delta k^2/k_0^2 \sim 10^{-2}$. As the IC phase moves into the bulk (as T is decreased), other harmonics, which make a negative contribution to the expression for k^2, grow. However, an analysis shows that k^2 cannot vanish, i.e., a continuous transformation of the incommensurate phase into the commensurate one, which we saw in the case D, cannot occur. Before k^2 vanishes, a first-order phase transition into the commensurate phase (where $k = 0$) with a jump in the wave vector will occur.

The phase diagram for the 1M functional in the (γ, T)

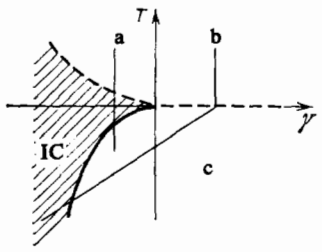

FIG. 17. Phase diagram for a functional without Lifshitz invariants. The broken line is the line of second-order transitions; the solid line is the line of first-order transitions; *a* and *b* are different thermodynamic paths.

plane was constructed by Michelson[27] in the one-harmonic approximation for the OP. It can be shown that inclusion of the harmonics does not change the qualitative structure of the diagram (Fig. 17), but only sharpens its boundary. Both lines, bounding the IC phase, remain parabolas, tangent to the line separating the initial and the *C* phases. All three of these lines converge at the Lifshitz point ($T = T_c, \gamma = 0$).

It follows from the diagram that for $\gamma < 0$, as the temperature is decreased, a sequence of phases IC→C (thermodynamic path *a*) appears. In many cases, the inverse sequence of phases C→IC is observed. It can appear for $\gamma > 0$, if the renormalization of γ due to the inclusion of an invariant of the form $-\delta\eta^2(d\eta/dz)^2$ in Φ is taken into account. Then the effective parameter

$$\tilde{\gamma} = \gamma - \delta\eta^2,$$

appears in Φ instead of γ and for sufficiently large δ in the condensed phase, where η increases as T is decreased, $\tilde{\gamma}$ will decrease with temperature and if it becomes negative, then a transition into the IC phase will occur. This will lead to a temperature-dependent wave vector in the IC phase:

$$k_0 = \sqrt{-\frac{\tilde{\gamma}}{2\alpha}} \sim \sqrt{T_c - T}. \tag{5.12}$$

Thus motion along the thermodynamic path δ could explain the reverse sequence of phase transitions C→IC.

We shall now study the functional (5.2) for a two-component OP (the functional 2M), describing the SS or TSW phases. We have a pair of complex conjugate minimization equations:

$$\left.\begin{aligned} \hat{L}\eta + 2u\eta^2\xi + nw\xi^{n-1} = 0, \\ \hat{L}\xi + 2u\xi^2\eta + nw\eta^{n-1} = 0. \end{aligned}\right\} \tag{5.13}$$

In the absence of anisotropy, these equations have exact solutions:

$$\eta = A_1 e^{ikz}, \quad \xi = A_1 e^{-ikz}. \tag{5.14}$$

The anisotropy generates multiple harmonics, whose form can be obtained using the Bogolyubov-Mitropol'skiĭ method[33] by studying the iterations of the equations with respect to the parameter w. We arrive at the following form of the harmonic series:

$$\eta = A_1 e^{ikz} + \sum_{p=1}^{\infty} \left(A_{pn+1} e^{i(pn+1)kz} + A_{-pn+1} e^{-i(pn-1)kz}\right), \tag{5.15}$$

where the amplitudes of the multiple harmonics have the following order of smallness:

$$A_{-pn+1} \sim w^p u^{p-1} A_1^{pn-1}, \quad A_{pn+1} \sim w^p u^p A_1^{pn+1}. \tag{5.16}$$

As can be seen from (5.15) and (4.13), in the case M the harmonics have the same structure as in the case D. This is natural, since in both cases the multiple harmonics appear due to the anisotropy, which has the same form in both cases.

In the approximation of the firt two harmonics, the nonequilibrium energy of the IC phase is equal to ($n > 4$)

$$\begin{aligned} \Phi_{IC} = {} & L(k) A_1^2 + L((n-1)k) A_{-n+1}^2 + L((n+1)k) A_{n+1}^2 \\ & + u(A_1^2 + A_{-n+1}^2 + A_{n+1}^2)^2 + 2uA_1^2 (A_{-n+1} + A_{n+1})^2 \\ & + (n-1) w A_1^{n-1} A_{-n+1}. \end{aligned} \tag{5.17}$$

Minimizing with respect to the amplitudes and the wave vector, we obtain

$$A_1 = \sqrt{-\frac{L(k)}{2u}}, \quad A_{-n+1} = -\frac{(n-1) w A_1^{n-1}}{L((n-1)k) + 4uA_1^2}, \tag{5.18}$$

$$A_{n+1} = -\frac{2uA_1^2 A_{-n+1}}{L((n+1)k) + 4uA_1^2},$$

$$k^2 = k_0^2 \left[1 - n(n-1)^2 (n-2) \frac{A_{n+1}^2}{A_1^2}\right]. \tag{5.19}$$

As in the case of the single-component OP, the wave vector cannot vanish, since the correction term in (5.19) is small. The type of phase diagram in the (γ, T) plane remains unchanged (Fig. 17).

Thus in systems without Lifshitz invariants the wave vector depends on the temperature through the dependence of the amplitudes of the multiple harmonics in the distribution of a one or two-component OP; in addition, the temperature-dependent term is small. The transition into the commensurate phase is a first-order phase transition with a jump in the wave vector. The amplitudes of the multiple harmonics are expressed as the corresponding power of the fundamental harmonic and grow with the depth of penetration into the condensed phase. These theoretical results correspond to the observed experimental data, and we shall analyze them in detail below.

Thus far we have assumed that the inhomogeneity of the structure arises along one direction in the crystal, i.e., the star of the wave vector **K** has two rays. The structures for which the wave vector lies in the symmetry plane and its star has more than two rays must be described by functionals with derivatives along several directions. The following functional (we shall call it $2M_2$) is a typical functional with a two-component OP for such situations:

$$\begin{aligned} \Phi = \int dx\, dy \Big[& r\eta\xi + u(\eta\xi)^2 + w(\eta^4 + \xi^4) \cdot \\ & + \gamma \left(\frac{\partial\eta}{\partial x}\frac{\partial\xi}{\partial x} + \frac{\partial\eta}{\partial y}\frac{\partial\xi}{\partial y}\right) \\ & + \alpha_1 \left(\frac{\partial^2\eta}{\partial x^2}\frac{\partial^2\xi}{\partial x^2} + \frac{\partial^2\eta}{\partial y^2}\frac{\partial^2\xi}{\partial y^2}\right) \\ & + \alpha_2 \left(\frac{\partial^2\eta}{\partial x^2}\frac{\partial^2\xi}{\partial y^2} + \frac{\partial^2\eta}{\partial y^2}\frac{\partial^2\xi}{\partial x^2}\right) + \alpha_3 \frac{\partial^2\eta}{\partial x\,\partial y}\frac{\partial^2\xi}{\partial x\,\partial y}\Big]. \end{aligned} \tag{5.20}$$

We shall study the modulated phases which it describes in the one-harmonic approximation:

$$\eta = A_1 e^{i(k_x x + k_y y)}, \quad \xi = \eta^*. \tag{5.21}$$

The corresponding nonequilibrium energy

$$\Phi_{\text{IC}} = [r + \gamma (k_x^2 + k_y^2) + \alpha_1 (k_x^4 + k_y^4) + (2\alpha_2 + \alpha_3) k_x^2 k_y^2] A_1^2 + u A_1^4 \tag{5.22}$$

must be minimized with respect to k_x, k_y, and A_1. The equations of minimization with respect to k_x and k_y have two types of solutions:

1) $k_x^2 = -\frac{\gamma_1}{2\alpha_1}, \quad k_y = 0$ or $k_x = 0, \quad k_y^2 = -\frac{\gamma_1}{2\alpha_1}$, (5.23)

2) $$k_x^2 = k_y^2 = -\frac{\gamma}{2\alpha_1 + 2\alpha_2 + \alpha_3}, \tag{5.24}$$

which are stable if $\gamma < 0$, $\alpha_2 + (\alpha_3/2) > \alpha_1$ and $\gamma < 0$, $\alpha_2 + (\alpha_3) < \alpha_1$, respectively. The symmetry of both solutions corresponds to a four-ray star of the wave vector. For the phase described by solution 1, the functional $2M_2$ transforms into the functional 2M with derivatives with respect to a single direction. The inclusion of other second-order invariants in the functional $2M_2$, for example,

$$\frac{\partial \eta}{\partial x}\frac{\partial \eta}{\partial y} - \frac{\partial \xi}{\partial x}\frac{\partial \xi}{\partial y},$$

leads to new solutions $k_x^2 \neq k_y^2$ with lower symmetry (see Sec. 7).

Relying on these typical functionals, we can analyze the phase transitions in specific materials. Before proceeding with the analysis, we shall complete our discussion of general theoretical questions by studying the effects of an external field. We shall examine, for definiteness, a system with a two-component OP, for example the SS structure, in a field applied perpendicular to the wave vector. The field can be regarded as a first-order anisotropy. The addition of the term

$$V_{\text{field}} = H (\eta + \xi) \tag{5.25}$$

to the functional (5.2) will lead to the following equation for η:

$$\alpha \frac{d^4\eta}{dz^4} - \gamma \frac{d^2\eta}{dz^2} + r\eta + 2u\eta^2\xi + H = 0 \tag{5.26}$$

and the complex conjugate equation for ξ. We have not included the natural crystalline anisotropy.

In the absence of a field, this nonlinear equation (pair of equations) has an exact solution—with one harmonic (5.14). In low fields, the asymptotic solution has the structure

$$\eta = \sum_{p=-\infty}^{\infty} A_p e^{ipkz}, \tag{5.27}$$

i.e., it contains all multiple harmonics without omissions; in addition, the smallness of the amplitudes is determined by the relations

$$A_1 \sim 1, \quad A_0, A_2 \sim H, \quad A_{-1}, A_3 \sim H^2, \ldots. \tag{5.28}$$

Using the method described above, we find the wave vector of the IC structure in a field:

$$k^2 = k_0^2 \left(1 - 12 \frac{A_2^2}{A_1^2}\right). \tag{5.29}$$

Its field dependence is determined by the amplitude of the first harmonic; in addition, $A_2^2/A_1^2 \sim H^2$.

Thus in low fields only some distortion of the spiral structure, described by the appearance of multiple harmonics and a decrease of the wave vector, occurs. In a very high critical field H_c the SS structure must evidently be destroyed and a state with uniform magnetization along the field appears. For $H > H_c$, the OP contains only the zeroth-order harmonic A_0, determined from the cubic equation

$$rA_0 + 2uA_0^3 + H = 0. \tag{5.30}$$

In subcritical fields $H < H_c$, an inhomogeneous state, usually called the FAN structure, appears. To find it, we shall use the other asymptotic limit: we shall seek the solution of Eq. (5.21) in the form of a series in powers of u, retaining the field-dependent term in the equation of the zeroth-order approximation, which has an exact solution of the form

$$\eta_0 = A_0 + A_1 e^{ikz} + A_{-1} e^{-ikz}. \tag{5.31}$$

The nonlinear term $\sim u\eta^2\xi$ generates new harmonics, which are found by minimizing the energy. The solution with the symmetry

$$A_1 = -A_{-1}, \quad A_2 = A_{-2}, \quad A_3 = -A_{-3}, \ldots, \tag{5.32}$$

has the lowest energy. We shall study this solution. For it, the amplitudes A_1, A_2, and A_3 are determined by the expressions

$$A_1^2 = -\frac{L(k) - 2uA_0^2}{6u}, \quad A_2 = \frac{4uA_1^2 A_0}{L(2k)}, \quad A_3 = \frac{4uA_1^3}{L(3k)}, \tag{5.33}$$

and the amplitude of the zeroth-order harmonic (the magnetization) satisfies the cubic equation

$$\left[r - \frac{2}{3} L(k)\right] A_0 + \frac{10}{3} u A_0^3 + H = 0 \quad (H < H_c). \tag{5.34}$$

This equation together with the equation $A_1 = 0$ determines in the (T, H) plane the line of the phase transition into the state with uniform magnetization. It is given in an implicit form by the pair of equations

$$-L(k) + 2uA_0^2 = 0, \quad rA_0 + 2uA_0^3 + H = 0. \tag{5.35}$$

The wave vector of the IC phase near this line depends on H and T through the amplitudes A_0 and A_1:

$$k^2 = k_0^2 \left[1 - \frac{192u^2}{L^2(2k)} A_1^2 A_0^2\right]. \tag{5.36}$$

The spatial distribution of the projections of the magnetic-moment density is determined by the expressions

$$M_x = \eta + \xi = 2A_0 + 4A_2 \cos 2kz + \ldots$$
$$M_y = i(\eta - \xi) = -4A_1 \sin kz - 4A_3 \sin 3kz + \ldots, \tag{5.37}$$

which define a parametric relationship between the components M_x and M_y (hodograph). In strong fields the hodograph represents an open curve (segment of a parabola), along which the tip of the vector $\mathbf{M}(z)$ moves in the case of a uniform displacement along the z axis. (Fig. 18). This describes the FAN structure. The FAN structure was determined previously in a manner such that the tip of the vector $\mathbf{M}(z)$ moves along a segment of a straight line perpendicular to the field. This straight line is transformed into a parabola

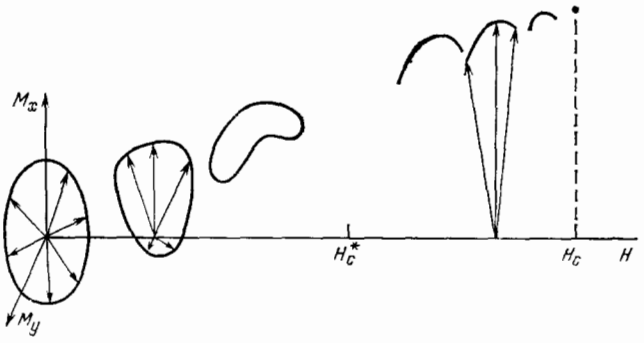

FIG. 18. Deformation of the spiral in an external magnetic field applied in the y direction.

by the term with the harmonic $\sim A_3$, which must be taken into account, since A_2 and A_3 are of the same order of magnitude. In weak fields, the hodograph is a closed curve. In an intermediate field $H_c^* \sim |L(0) - 2L(k)|A_1$, the topology of the hodograph changes, and this point is probably a phase-transition point.

Relying on the results of the phenomenological theory presented in Secs. 4 and 5, we shall analyze below the experimental data obtained by neutron-diffraction analysis of the modulated magnetic phases in crystals as well as the phase transitions between them. The study of the magnetic phases in two classes of materials is of special interest: in rare-earth metals and in tetragonal crystals of the type $TbAg_2$ with the symmetry group D_{4h}^{17}, since each of these classes has a set of members which have the same crystalline structure, but different magnetic structures.

6. ANALYSIS OF MAGNETIC PHASE TRANSITIONS IN RARE-EARTH METALS

Rare-earth metals belonging to the heavy group have LSW and SS structures with the wave vector $[00\mu]$, where μ depends on the temperature, but remains small, assuming values near 0.28.[9,34] We can therefore speak about modulation of structures with the wave vector $\mathbf{K}_0 = 0$. The observed structures are classified according to the irreducible representations (IR) with $\mathbf{k} = 0$ of the group D_{6h}^4 (Table II). It turns out here that the LSW structure with the spins oriented along the principal axis of the crystal is described by the one-dimensional representation τ_3, and the SS structure with spins lying in the basal plane is described by the two-dimensional representation τ_q (the nomenclature everywhere follows Kovalev[35]).

In the classification of modulated structures according to the irreducible representations of the symmetry point, the distinction between the IC and C phases is lost, since the LSW structure and the ferromagnetic structure F (with the spins oriented along the hexagonal axis) are characterized by the same IR τ_3, while the spiral structure SS and the structure F (with the spins oriented in the basal plane)are characterized by the IR τ_9.

It is not difficult to show that the phase transition into the LSW structure is described by a functional of the type 1M, while the transition into the SS structure is described by the functional 2M, where the order of the anisotropy is $n = 6$. In the last case, the functional describes both magnetic transitions, including the transition SS→F from the C into the IC phase, observed in Tb and Dy. The phase transition SS→FS in Ho is of an entirely different type, since it occurs between phases with different symmetry. The cascade of phase transitions in Er must be described by two coupled OR: a one-component or (symmetry τ_3) and a two-component or (symmetry τ_9). If an SS structure did not occur in this metal, then the phase transition LSW→F from the C into the IC structure according to the representation τ_3 would occur in a pure form. The second stage of this cascade—the transition LSW + SS→FS—is a transition from the IC into the C structure (with respect to the S_z component of the spins). Both phases are described by the same representation $\tau_3 + \tau_9$. All transitions from the IC phase into the C phase in rare-earth metals are first-order transitions. As we can see, they must all be described by Michelson's phase diagram (Fig. 17) for $\gamma < 0$. It should be kept in mind that the parameter γ for rare-earth metals depends on the temperature as a result of a peculiar mechanism for the appearance of a magnetic inhomogeneity in them: via the interaction of the atomic spins with the conduction electrons. As a result of this, the thermodynamic path with a change in temperature is not the straight line a in Fig. 17, but rather some complicated curve. The wave vector of the LSW or SS structure depends on the temperature. This dependence is determined, on the one hand, by the intrinsic dependence of the parameter $\gamma(T)$ and, on the other, by the contribution of the multiple harmonics. It would be of great interest to separate these two contributions.

Since magnetic phase transitions in rare-earth metals are described by the functionals 1M and 2M already studied above, all phenomena examined theoretically in the preceding section can appear in them. On of them is the appearance of higher-order satellites, corresponding to higher-order harmonics of the OP arising due to the anisotropy. In neutron-diffraction studies of Ho in the SS phase, fifth- and seventh-order satellites, corresponding to spin projections in the basal plane, are indeed observed.[43] Precisely such satellites should occur (see (5.15)), since in the presence of hexagonal symmetry the order of the anisotropy in the basal plane is $n = 6$ and, therefore, $n \pm 1 = 5$ and 7. In Er in the LSW phase, odd-order satellites are observed (Fig. 6) in accordance with the theory, since the projections of the spins on the hexagonal axis feel the second-order anisotropy ($n = 2$).

Third- and fifth-order satellites, arising due to the spin projections on the basal plane, are observed in the intermediate modulated phase (CS) in Er. The third-order satellites cannot be explained by anisotropy in this plane, but their existence can be understood based on the functional 1M + 2M with coupled OP.[37] Indeed, we shall write for Er the energy functional in the exchange approximation taking into account the uniaxial anisotropy:

$$\Phi = \int dz \left[r\mathbf{M}^2 + u\mathbf{M}^4 + \gamma \left(\frac{d\mathbf{M}}{dz} \right)^2 + \alpha \left(\frac{d^2\mathbf{M}}{dz^2} \right)^2 - KM_z^2 \right]. \quad (6.1)$$

In the Er crystal, M_z transforms according to the one-dimensional IR of the group D_{6h}^4, while M_x and M_y transform according to the two-dimensional IR. We can thus introduce two OP: a single-component OP ζ and a two-component OP (η, ξ)

$$\zeta = M_z; \quad \eta = M_x + iM_y, \quad \xi = M_x - iM_y. \tag{6.2}$$

In these terms Φ is written as a functional of two interacting OP:

$$\Phi = \int dz \left\{ r_1\zeta^2 + r_2(\eta\xi) + \gamma\left[\left(\frac{d\xi}{dz}\right)^2 + \frac{d\eta}{dz}\frac{d\xi}{dz}\right] + \alpha\left[\left(\frac{d^2\zeta}{dz^2}\right)^2 + \frac{d^2\eta}{dz^2}\frac{d^2\xi}{dz^2}\right] + u(\zeta^2 + \eta\xi)^2 \right\}. \tag{6.3}$$

The quantities r_1 and r_2 differ by an amount K—the energy of the uniaxial anisotropy, which splits the magnetic phase transition: first the ζ (LSW) ordering and then the (η, ξ) (SS) ordering appears.

In the LSW phase, the OP contains odd harmonics (see (5.5)):

$$\zeta = \sum_p A_p \cos(pkz), \qquad p = 1, 3, 5, \ldots . \tag{6.4}$$

In the CS phase, an ordering of the M_x and M_y projections, described by the OP

$$\eta = \sum_p (B_p e^{ipkz} + B_{-p} e^{-ipkz}), \tag{6.5}$$

with a set of multiple harmonics whose amplitudes must be determined by minimizing the energy, also appears. If the anisotropy in the basal plane is neglected, then multiple harmonics are not present in the distribution (6.5). They appear due to the coupling with the OP ζ; in addition, their amplitudes are expressed in terms of the amplitude of the fundamental harmonic in ζ:

$$B_3 \sim uA_1^3B_1, \quad B_5 \sim u^2A_1^4B_1, \ \ldots . \tag{6.6}$$

An analysis of the exact expressions for the amplitudes B_3 and B_5 shows that they pass through a maximum as the temperature varies from T_2 to T_3.[37]

Commensurability effects are manifested in the temperature dependence of the wave vector of some rare-earth metals. Thus, for example, in Ho as the temperature is decreased, μ varies from 0.28 and locks when the value $\mu = 1/6$ is reached. A commensurate FS phase appears at the corresponding temperature. To describe this phenomenon, it is necessary to construct a functional directly for the wave vector $\mathbf{K} = [0\ 0\ 1/6]$. The star $\{\mathbf{k}\}$ of the wave vector $[0\ 0\ \mu]$ has two rays, and the SS structure is described by a two-dimensional IR τ_5 of the group $G_{\mathbf{k}}$. The corresponding IR for the space group D_{6h}^4 is four-dimensional. We denote the basis functions by η_1 and η_2 for one of its rays $\mathbf{k}$ and by ξ_1 and ξ_2 for the other ray $-\mathbf{k}$. The full potential, taking into account the sixth-order invariants for the commensurate vector $\mathbf{K}_0$, is equal to

$$\begin{aligned}\Phi = \int dz \Big[& r(\eta_1\xi_2 + \eta_2\xi_1) + u(\eta_1^2\xi_2^2 + \eta_2^2\xi_1^2) + u'\eta_1\eta_2\xi_1\xi_2 \\ & + i\sigma\left(\eta_1\frac{d\xi_2}{dz} - \xi_1\frac{d\eta_2}{dz} + \eta_2\frac{d\xi_1}{dz} - \xi_2\frac{d\eta_1}{dz}\right) \\ & + \gamma\left(\frac{d\eta_1}{dz}\frac{d\xi_2}{dz} + \frac{d\eta_2}{dz}\frac{d\xi_1}{dz}\right) \\ & + w(\eta_1^6 + \eta_2^6 + \xi_1^6 + \xi_2^6) + w'(\eta_1^3\xi_2^3 + \eta_2^3\xi_1^3) + w''(\eta_1^3\eta_2^3 + \xi_1^3\xi_2^3) \\ & + w'''(\eta_1^3\xi_1^3 + \eta_2^3\xi_2^3) + w''''(\eta_1\xi_2(\eta_2\xi_1)^2 + \eta_2\xi_1(\eta_1\xi_2)^2)\Big].\end{aligned} \tag{6.7}$$

The appearance of a linear Lifshitz invariant should not be surprising, since the expansion (6.7) is written not for the symmetrical point of the Brillouin zone $\mathbf{K}_0 = 0$ (for which the functional Φ would be 2M), but rather for the line $\mathbf{K}_0 = [0\ 0\ \mu]$, where the symmetry is already different. On this line, the form of the first five invariants does not depend on μ, but the form of the anisotropic terms (proportional to $w, w', \ldots$) is specific to the particular value of $\mu = 1/6$. The functional (6.7) describes the system near the wave vector $[0\ 0\ 1/6]$ and contains the corresponding commensurability effects.

The simple spiral is described by a pair of nonzero values of the OP: (η_1, ξ_2) and (η_2, ξ_1) (right- and left-handed spirals). In the presence of all four components of the OP, the two differently polarized spirals are superposed. Consider, for example, the phase (η_1, ξ_2). Then the general expression (6.7) will simplify (the indices for η and ξ are omitted):

$$\Phi = \int dz \left[r(\eta\xi) + u(\eta\xi)^2 + w(\eta^6 + \xi^6) + i\sigma\left(\eta\frac{d\xi}{dz} - \xi\frac{d\eta}{dz}\right) + \gamma\frac{d\eta}{dz}\frac{d\xi}{dz}\right], \tag{6.8}$$

and we therefore arrive at the functional (D) for $n = 6$. The locking of the wave vector, which it describes on the value $[0\ 0\ 1/6]$ is well known. The typical behavior of the wave vector is indeed observed near the second phase-transition point in Ho. The locking of the wave vector on $\mu = 2/7$ in Tm (with the help of the anisotropic term $w(\eta^{14} + \xi^{14})$) and on $\mu = 1/4$ in Er are described analogously.

Thus the entire picture of phase transitions in rare-earth metals and the structure of their phases can be explained within the framework of the phenomenological theory. It would be interesting to obtain the effective Ginzburg-Landau functional from microscopic models and to express thereby the phenomenological parameters of the functional in terms of the microscopic properties of the metal.

7. MAGNETIC PHASE TRANSITIONS IN CRYSTALS OF THE TYPE $TbAg_2$

Compounds of the type $TbAg_2$ form another extensive class of materials with an isomorphic crystalline structure and diverse modulated magnetic phases.

Information on the magnetic structure of these materials and all the required references can be found in the handbook of Ref. 5. In the $TbAg_2$ crystal, the magnetic Tb atoms occupy the 2 (*a*) position of the space group D_{4h}^{17}–$I4/mmm$ and the nonmagnetic atoms occupy the 4 (*e*) position. Thus the magnetic atoms form a body-centered tetragonal Bravais

lattice with one atom per primitive cell.

As can be seen from Table III, the diverse magnetic structures in crystals of this class are long-periodic modulations of antiferromagnetic structures with the following wave vectors:

$$\mathbf{K}_0 = 0, \qquad \text{star} \quad \{\mathbf{k}_{14}\}, \tag{7.1}$$

$$\mathbf{K}_0 = \frac{2\pi}{c}[0\,0\,1] = \frac{1}{2}(\mathbf{b}_1 + \mathbf{b}_2 - \mathbf{b}_3), \qquad \text{star} \quad \{\mathbf{k}_{15}\}, \tag{7.2}$$

$$\mathbf{K}_0 = \frac{2\pi}{a}\left[\frac{1}{2}\,\frac{1}{2}\,0\right] = \frac{1}{2}\,\mathbf{b}_3, \qquad \text{star} \quad \{\mathbf{k}_{13}\}. \tag{7.3}$$

The transition from the diffraction notation for the wave vectors to the notation adopted in the theory of representations of space groups is made with the help of the shortest vectors of the primitive reciprocal cell of the body-centered tetragonal crystal:

$$\mathbf{b}_1 = 2\pi\left[0\,\frac{1}{a}\,\frac{1}{c}\right], \quad \mathbf{b}_2 = 2\pi\left[\frac{1}{a}\,0\,\frac{1}{c}\right],$$

$$\mathbf{b}_3 = 2\pi\left[\frac{1}{a}\,\frac{1}{a}\,0\right].$$

In magnetic structures associated with one-ray stars $\{\mathbf{k}_{14}\}$ and $\{\mathbf{k}_{15}\}$, the spins lie in the basal plane and therefore transform according to a two-dimensional representation. The only two-dimensional representation for both stars is τ_9. For the star $\{\mathbf{k}_{13}\}$, all IR are one-dimensional along a ray and two-dimensional for the entire space group. In the magnetic representation $d^{\mathbf{k}}_{M}$ there are three IR on the magnetic atoms of the crystal:

$$d^{\mathbf{k}}_{M} = \tau_3 + \tau_5 + \tau_7 \qquad \{\mathbf{k}_{13}\}. \tag{7.4}$$

The atomic components of the pseudovector basis functions of all required IR are presented in Table IV.

We begin with an analysis of the magnetic phases, corresponding to modulation of the structure with $\mathbf{k} = 0$. For $MnAu_2$, the functional 2M with $n = 4$ corresponds to the two-dimensional representation τ_9 of the star $\{\mathbf{k}_{14}\}$. For the compound $PrCo_2Ge_2$, a functional of the form 1M corresponds to the one-dimensional representation τ_3 of the star $\{\mathbf{k}_{14}\}$.

We now go on to compounds described by the two-ray star $\{\mathbf{k}_{13}\}$. We denote the mixing coefficients of the basis functions for the rays $\mathbf{k}_1 = [1/2\ 1/2\ 0]$ and $\mathbf{k}_2 = [1/2\ 1/2\ 0]$ by η and ξ, respectively. They are the order parameters. For the IR τ_7, we obtain

$$\begin{aligned}\Phi = \int \mathrm{d}\mathbf{r}\,[&r(\eta^2+\xi^2) + u(\eta^4+\xi^4) + v\eta^2\xi^2 \\ &+ \gamma_1'(\eta_x^2+\eta_y^2+\xi_x^2+\xi_y^2) \\ &+ \gamma_2'(\eta_x\eta_y - \xi_x\xi_y) + \alpha_1'(\eta_{xx}^2+\eta_{yy}^2+\xi_{xx}^2+\xi_{yy}^2) \\ &+ \alpha_2'(\eta_{xx}\eta_{yy}+\xi_{xx}\xi_{yy}) \\ &+ \alpha_3'(\eta_{xy}^2+\xi_{xy}^2) + \alpha_4'[(\eta_{xx}+\eta_{yy})\eta_{xy} - (\xi_{xx}+\xi_{yy})\xi_{xy}]].\end{aligned} \tag{7.5}$$

We shall not write out the invariants containing the derivatives with respect to z, since modulation is observed only along a direction in the basal plane. Invariants which are linear with respect to the derivatives are absent (they are absent for all IR contained in Table IV). For magnetic structures in $TbAu_2$, DyC_2, $DyAg_2$, and $DyAu_2$ with the wave vector $[\mu\,\mu\,0]$, it is necessary to transform to the derivatives with respect to l and t along the [110] and [1$\bar{1}$0] directions, which is achieved with the help of the linear transformation

$$l = x + y, \quad t = x - y. \tag{7.6}$$

In these variables, the functional (7.5) is diagonalized with respect to the derivatives and assumes the form

$$\begin{aligned}\Phi = \int \mathrm{d}l\,\mathrm{d}t\,\{&r(\eta^2+\xi^2) + u(\eta^4+\xi^4) + v\eta^2\xi^2 \\ &+ \gamma_1(\eta_l^2+\xi_t^2) + \gamma_2(\eta_t^2+\xi_l^2) \\ &+ \alpha_1(\eta_{ll}^2+\xi_{tt}^2) + \alpha_2(\eta_{tt}^2+\xi_{ll}^2) \\ &+ \alpha_3(\eta_{ll}\eta_{tt}+\xi_{ll}\xi_{tt}) + \alpha_4(\eta_{lt}^2+\xi_{lt}^2)\},\end{aligned} \tag{7.7}$$

whence it is evident that both directions [110] and [1$\bar{1}$0] are equivalent. In the interpretation of magnetic structures with multiray stars, it is assumed that a single-ray structure is realized. We shall therefore set one of the OP in (7.7), for example ξ, equal to zero. If it is assumed that the constants γ_1 and γ_2 have different signs, then it is energetically favorable for structures modulated only in a single direction to appear. Thus it must be assumed that in the compounds $TbAu_2$, DyC_2, $DyAg_2$, and $DyAu_2$

$$\xi = 0, \quad \gamma_1 < 0, \quad \gamma_2 > 0, \tag{7.8}$$

in order for their observed magnetic structure to be realized. Here, for these specific materials, the Ginzburg-Landau functional becomes a one-dimensional and an effectively single-component functional:

$$\Phi = \int \mathrm{d}l\,(r\eta^2 + u\eta^4 + \gamma_1\eta_l^2 + \alpha_1\eta_{ll}^2). \tag{7.9}$$

It essentially coincides with the 1M functional. The transi-

TABLE IV. Basis functions of irreducible representations of the group D_{4h}^{17} for one magnetic atom in the primitive cell of the crystal.

$\{\mathbf{k}_{14}\}$	$\{\mathbf{k}_{15}\}$		$\{\mathbf{k}_{13}\}$		
			τ_3	τ_5	τ_7
1	$\mathbf{m}_9\,(1-i0)$	$\mathbf{k}_1$	$\mathbf{m}_3\,(1\bar{1}0)$	$\mathbf{m}_5\,(110)$	$\mathbf{m}_7\,(001)$
2	$(1i0)$	$\mathbf{k}_2$	(110)	$(\bar{1}10)$	(001)

tion, observed in these compounds, into the commensurate structure accompanying a change in the wave vector $[\mu\mu 0] \to [1/2\ 1/2\ 0]$ corresponds to the thermodynamic path a in the phase diagram (see Fig. 17).

In the two other IR τ_3 and τ_5 of $\{\mathbf{k}_{13}\}$, the form of the invariants in the approximation adopted is the same as for the IR τ_7, so that the functional (4.7) corresponds to all three IR of the star $\{\mathbf{k}_{13}\}$.

In the $HoAg_2$, $ErAu_2$, and $ErAg_2$ crystals, a mixed phase, characterized by the pair of Ir of the star $\{\mathbf{k}_{13}\}$ appears. For systems of two interacting OP (η_1, ξ_1) and (η_2, ξ_2) the functional consists of three terms:

$$\Phi = \Phi_1 + \Phi_2 + \Phi_{12}, \tag{7.10}$$

where Φ_1 is given by expression (5.2) for η_1 and ξ_1 and by the same expression for η_2 and ξ_2, but with different values of the parameters r, u, w, ... The mixed term for all pairs of IR has the form

$$\Phi_{12} = \int dl\, dt\, [v_1 (\eta_1^2\eta_2^2 + \xi_1^2\xi_2^2) + v_2 (\eta_1^2\xi_2^2 + \eta_2^2\xi_1^2)]. \tag{7.11}$$

Thus sequences of phase transitions in the indicated compounds are described by a one-dimensional functional of two coupled single-component OP:

$$\Phi = \int dl\, (r_1\eta_1^2 + u_1\eta_1^4 + \gamma_1\eta_1^2{}_{,l} + \alpha_1\eta_1^2{}_{,ll} + r_2\eta_2^2 + u_2\eta_2^4 + \gamma_2\eta_2^2{}_{,l} + \alpha_2\eta_2^2{}_{,ll} + v\eta_1^2\eta_2^2) \tag{7.12}$$

with the following conditions on the parameters γ_1 and γ_2: $\gamma_1 < 0$, $\gamma_2 < 0$ ($HoAg_2$), $\gamma_1 < 0$, $\gamma_2 > 0$ ($HoAu_2$, $ErAu_2$). The neutron-diffraction data for $ErAg_2$ show that the commensurate and incommensurate components of the same OP coexist in the low-temperature phase. The functional (7.12) does not admit the existence of such a phase. It is possible that a domain magnetic structure is manifested experimentally.

We now go on to the compounds HoC_2 and TbC_2. The symmetry τ_9 of $\{\mathbf{k}_{15}\}$ corresponds to a functional with an inhomogeneity in the x, y plane:

$$\begin{aligned}\Phi = \int dx\, dy\, \{&r(\eta\xi) + u(\eta\xi)^2 + w(\eta^4 + \xi^4) \\ &+ \gamma_1(\eta_x\xi_x + \eta_y\xi_y) + \gamma_2(\eta_x^2 + \xi_x^2 - \eta_y^2 - \xi_y^2) \\ &+ i\gamma_3(\eta_x\eta_y - \xi_x\xi_y) \\ &+ \alpha_1(\eta_{xx}\xi_{xx} + \eta_{yy}\xi_{yy}) \\ &+ \alpha_2(\eta_{xx}\xi_{yy} + \eta_{yy}\xi_{xx}) + \alpha_3\eta_{xy}\xi_{xy} \\ &+ \alpha_4(\eta_{xx}^2 - \eta_{yy}^2 + \xi_{xx}^2 - \xi_{yy}^2) \\ &+ \alpha_5[\eta_{xy}(\eta_{xx} + \eta_{yy}) - \xi_{xy}(\xi_{xx} + \xi_{yy})]\}.\end{aligned} \tag{7.13}$$

It contains additional inhomogeneous invariants with respect to the model functional $2M_2$ (5.20), which we examined above. The functional (5.20) leads to symmetrical solutions (5.24), which describe the magnetic structures in HoC_2 and TbC_2. Additional inhomogeneous invariants lead to nonsymmetrical solutions, for which $k_x^2 \neq k_y^2$. It is easy to see that as the temperature is decreased, the inhomogeneous second-order anisotropy (invariants $\sim\gamma_2$ and $\sim\gamma_3$) lead to the appearance of multiple harmonics of odd orders. Their inclusion leads to a temperature dependence of the magnitude and orientation of the wave vector $\mathbf{k}$.

In HoC_2 and TbC_2 crystals, for which the functional (7.13) was obtained, SS structures with the wave vector $\mathbf{k} = (k_x\ 0\ 0)$, corresponding to a symmetrical solution of the type (5.23), are realized. In a number of substances, however, modulated structures with a wave vector $\mathbf{k}$ lying in the common position (see Table I) appear. The mechanisms of the inhomogeneous anisotropy of the type which we just examined are apparently responsible for this.

8. EFFECT OF EXTERNAL FIELDS ON THE WAVE VECTOR OF INCOMMENSURATE PHASES

We have already examined the change of the wave vector of a simple spiral in a magnetic field applied in the plane of rotation of the spins, i.e., in a direction perpendicular to the wave vector. The magnitude of the wave vector decreased as the field increased (in both cases, with and without Lifshitz invariants in the free energy), but the orientation of the vector remained unchanged with a fixed geometry. The analysis performed can be extended along two directions: for magnetic fields oriented arbitrarily with respect to the wave vector and also for other physical actions applied to the system, for example, deformation.[39-41,61]

If the field is applied in an arbitrary direction with respect to the wave vector of the incommensurate structure, oriented, for example, in the z direction, then the symmetry can sometimes admit gradient invariants along a different direction, which will lead to an instability of the phase with the initial orientation of the wave vector. The instability appears, for example, if invariants of the form

$$\lambda H_x H_z i \left(\eta\frac{\partial\xi}{\partial x} - \xi\frac{\partial\eta}{\partial x}\right). \tag{8.1}$$

are admitted. The appearance of the indicated invariant will cause the wave vector to be deflected in the x direction. The nature of this deflection depends on whether the structure is commensurate or incommensurate. If it is commensurate, then the functional Φ contains an energy of commensurability, described by the invariant $w(\eta^n + \xi^n)$. In the approximation of a constant modulus ρ of the OP, the problem of the equilibrium distribution of OP in the field is evidently described by the functional

$$\Phi = \int dz \left[\gamma\rho^2\left(\frac{d\varphi}{dz}\right)^2 + 2\lambda H_x H_z\rho^2\frac{d\varphi}{dz} + 2w\rho^n\cos n\varphi\right], \tag{8.2}$$

which essentially coincides with the functional (4.2) which we have already examined. The solution of the corresponding variational problem has the form[40] (see (4.5))

$$\varphi(x) = \begin{cases} \text{const}, & H_x H_z \leqslant H_c^2, \\ \dfrac{2}{n}\,\mathrm{am}(qx, \varkappa), & H_x H_z \geqslant H_c^2, \end{cases} \tag{8.3}$$

where

$$H_c^2 = \frac{4}{\pi\lambda}\sqrt{w\gamma}\rho^{(n-2)/2}, \quad q = \frac{n}{\varkappa}\sqrt{\frac{w}{\gamma}}\rho^{(n-2)/2}. \tag{8.4}$$

Thus there exists a threshold value of the quantity $H_x H_z$ below which the commensurate structure is preserved (this

could be the usual ferro- or antiferromagnetic structure or a modulated structure with a commensurate wave vector) due to the energy of commensurability. When the threshold is exceeded, modulation appears in the system in the x direction, as described by Eq. (8.3). It is evident from this equation that if the starting structure is incommensurate, then the modulation in the x direction is induced by an obliquely oriented field in a nonthreshold manner.

We shall indicate other fundamental possibilities for magnetic-field control of the wave vector in terms of invariants of the type

$$c_{\alpha\beta}H_\alpha H_\beta\eta^2 + \text{c.c.}, \tag{8.5}$$

$$d_{\alpha\beta}H_\alpha H_\beta \frac{d\eta}{dz}\frac{d\xi}{dz}. \tag{8.6}$$

The first of these possibilities for a modulated antiferromagnet, in which the modulation is due to a Lifshitz invariant, was pointed out in Ref. 26. If the field is applied in the plane of rotation of the spins, which is perpendicular to the wave vector of the antiferromagnet $\mathbf{K}_0$, then the invariant (8.5) describes the field-induced second-order anisotropy, which, according to the mechanism described in Sec. 4, can change the magnitude of the wave vector $\mathbf{K}$ up to the commensurate value $\mathbf{K}_0$. An invariant of the type (8.6) leads to a direct change in the constant γ in the general functional (3.1)–(3.2), which determines the magnitude of the wave vector according to one of the expressions (3.4). A generalized expression of the type

$$D_{\alpha\beta\gamma\delta}H_\alpha H_\beta \frac{\partial\eta}{\partial x^\gamma}\frac{\partial\xi}{\partial x^\delta} \tag{8.7}$$

contains the possibility of changing not only the magnitude of the wave vector, but also its orientation. It is clear that a field oriented obliquely with respect to the vector $\mathbf{K}_0$ must unavoidably rotate it, since the symmetry of the system (crystal + field) no longer reflects the "good" orientation of the wave vector. For an incommensurate structure, this rotation will occur in an arbitrarily weak field, while for a commensurate structure it must begin at some threshold value.

Analogous effects must also arise in the presence of other external actions on the system, for example, in the presence of deformation. Their role can be demonstrated by one good example. In the cubic crystal $ZnCr_2Se_4$, a spiral magnetic structure SS with the wave vector oriented along the edge of a cube, close to the vector $\mathbf{K}_0 = (0\,0\,1/2)$, arises at $T_N = 21$K.[10] The magnetic phase transition here is a first-order transition, and it is accompanied by the appearance of spontaneous deformation along the wave vector. As the temperature is decreased, the wave vector of the spiral changes strictly proportionally to the change in the ratio of the lattice constants c/a, characterizing the magnitude of the deformation (Fig. 19). It can be shown that this linear relationship between K and c/a arises from the symmetry of the system. $ZnCr_2Se_4$ has the spinel structure and the magnetic Cr atoms occupy the 16 (d) positions of the space group O_h^7. The magnetic modes of the antiferromagnetic structure with $\mathbf{K}_0 = (0\,0\,1/2)$ were calculated in Ref. 4, and from a comparison of these modes with the observed SS structure it follows that the latter represents a weak modulation of the collinear antiferromagnetic structure, described by two two-dimensional irreducible representations τ_1 and τ_2 of the group of the vector $\mathbf{K}_0$. Denoting the components of the OP transforming according to τ_1 by (η_1, η_2) and those transforming according to τ_2 by (ξ_1, ξ_2), we can obtain a functional Φ for the four-component OP. It contains a Lifshitz invariant which includes the basis functions of both irreducible representations:

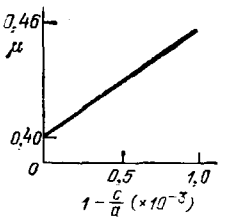

FIG. 19. Relationship between the wave vector of the spiral structure in $ZnCr_2Se_4$ and the spontaneous deformation of the lattice.

$$\sigma\left(\xi_1\frac{d\eta_1}{dz} - \eta_1\frac{d\xi_1}{dz} + \eta_2\frac{d\xi_2}{dz} - \xi_2\frac{d\eta_2}{dz}\right). \tag{8.8}$$

There also exist two invariants which contain the component of the strain tensor ε_{zz}:

$$\beta_1\left(\xi_1\frac{d\eta_1}{dz} - \xi_2\frac{d\eta_2}{dz}\right)\varepsilon_{zz} + \beta_2\left(\eta_2\frac{d\xi_2}{dz} - \eta_1\frac{d\xi_1}{dz}\right)\varepsilon_{zz}. \tag{8.9}$$

The SS structure, observed in $ZnCr_2Se_4$, is described by the following definition of the components of the OP:

$$\eta_1 = \eta\sin kz, \quad \xi_1 = \eta\cos kz, \quad \eta_2 = \xi_2 = 0.$$

For the full class of solutions, the problem of determining the equilibrium structure reduces to the minimization of a functional with a one-component OP interacting with the deformation ε_{zz}:

$$\Phi_{SS} = r\eta^2 + u\eta^4 + \sigma k\eta^2 + \gamma k^2\eta^2 + L\varepsilon_{zz}^2 + \delta\eta^2\varepsilon_{zz} + \beta k\eta^2\varepsilon_{zz}, \tag{8.10}$$

whence we obtain the magnitude of the wave vector k and of the spontaneous strain ε_{zz}^0:

$$k = -\frac{\sigma + \beta\varepsilon_{zz}^0}{2\gamma}, \tag{8.11}$$

$$\varepsilon_{zz}^0 = -\frac{1}{2L}\left(\delta - \frac{\sigma}{2\gamma}\beta\right)\eta^2, \quad \eta^2 \approx -\frac{r}{2u}. \tag{8.12}$$

The relation (8.11) demonstrates the linear relationship between k and ε_{zz}^0, arising due to the invariants (8.8) and (8.9)

Elimination of the quantity ε_{zz} from the expression (8.10) leads to the renormalization

$$u \to u - \frac{1}{2L}\left(\delta - \frac{\sigma}{2\gamma}\beta\right)^2,$$

as a result of which u can become negative, and this will lead to a first-order phase transition. A first-order phase transition is observed experimentally, but no unequivocal conclusion concerning the indicated mechanism can be drawn, since in the presence of magnetostriction the magnetic fluctuations, which were ignored in this calculation, also cause the second-order phase transition to change into a first-order transition.[42]

It should be noted that the crystal $ZnCr_2Se_4$ is a rare

example of a crystal in which modulations of the magnetic structure arise due to the Lifshitz invariants. In spite of the high symmetry of this crystal, the invariant linear with respect to the gradients exists due to the participation of two irreducible representations. As is well known, such invariants describe the energy of small relativistic interactions, so that the modulations caused by them must also be small. Indeed, in $ZnCr_2Se_4$ the angle of rotation of the spins in two neighboring planes of the crystal is equal to 42° at $T = 4.2$ K.[10] If this angle were exactly equal to 45°, then this would correspond to an antiferromagnetic structure with the wave vector $\mathbf{K}_0 = (0\ 0\ 1/2)$, whence it is clear that the modulation vector $\mathbf{k}$ is very small. Another example of modulated magnetic structures which arise due to Lifshitz invariants are the two isomorphic compounds MnSi and FeGe, which have the space group T^4, which does not have a center of inversion. In both crystals, the modulation vector is also very small.[22,23] This behavior is also observed in purely structural modulations of the crystals.

CONCLUSIONS

The extensive experimental data on the modulated magnetic structures of crystals and on the phase transitions between them can be understood on the basis of the minimization of the Ginzburg-Landau functionals for an inhomogeneous distribution of the order parameter. Phenomena such as the temperature and field dependence of the wave vector, the appearance of higher-order satellites in the neutron-diffraction patterns, and the appearance of a sequence of commensurate and incommensurate phases are manifestations of the effects of nonlinearity in the system and are described by the solutions of nonlinear differential equations for the order parameter, minimizing the free energy. Such a functional can be constructed for each specific magnetic phase transition analogously to the method demonstrated here on a number of examples.

It would be useful to make further progress in the physics of modulated phases in two directions. On the one hand, the parameters of the phenomenological Ginzburg-Landau functional for specific materials could be determined by studying different properties of magnetic phases experimentally and, on the other, this functional could be derived from microscopic models, thereby leading to a microscopic interpretation of these parameters. The construction of phase diagrams of magnetic states, for example, in the temperature–magnetic-field plane, as was done recently for MnP, is an important integral part of this program.

The other direction is to study the effects of commensurability, i.e., anomalies of the physical properties accompanying the passage of the wave vector through a commensurate value. Careful magnetic, acoustical, and dilatometric measurements have shown that such anomalies do in fact exist where neutron-diffraction experiments did not previously reveal them. An example is the latest study of holmium.[43] It would be interesting to check directly the solution picture of the incommensurate phase by neutron-diffraction analysis. Possible candidates for checking the corresponding theory of diffraction, developed in Sec. 4, are the crystals MnSi and FeGe, in which the existence of spiral structures is due to Lifshitz invariants. The prediction of chaotic incommensurate structures must also be checked experimentally.[3,44]

In this review, we restricted our attention to the static properties of modulated magnetic phases. The dynamics of commensurate and incommensurate structures has specific features, in which commensurability effects are once again manifested. The spectrum of the fluctuations of modulated structures was established analytically for systems with Lifshitz invariants[45,46] in the approximation of a constant modulus of the order parameter.[27] The corresponding excitations—phasons—are studied with the help of light and neutron scattering in nonmagnetic crystals in the vicinity of structural phase transitions.[47,2] For magnetic modulated phases, such experimental studies have not yet begun. The problem of the theoretical analysis of the spectra of fluctuations of modulated structures in systems without Lifshitz invariants has also not been studied. We note that for the overwhelming majority of magnetically ordered crystals with modulated structures, the symmetry does not admit linear Lifshitz invariants, so that the spectrum of the fluctuations of such systems remains completely uninvestigated.

[1]A. Herpin and P. Meriel, J. Phys. (Paris) **22**, 337 (1961).
[2]J. Petzelt in: Phase Transitions, Gordon and Breach, NY (1981), Vol. 2, p. 155.
[3]P. Bak, Rept. Progr. Phys. **45**, 587 (1982).
[4]Yu. A. Izyumov, V. E. Naĭsh, and R. P. Ozerov, Neĭtronografiya magnetikov (Neutron-Diffraction Analysis of Magnetic Materials), Atomizdat, Moscow (1981).
[5]A. Oles, F. Kajzar, M. Kucab, and W. Sikora, Magnetic Structures Determined by Neutron Diffraction, Krakov, Warszawa (1976).
[6]W. Schafer and G. Will, J. Phys. Chem. Sol. **40**, 239 (1979).
[7]P. Bak and M. H. Jensen, J. Phys. Ser. C **13**, L881 (1980).
[8]M. L. Plumer and M. B. Walker, Ibid. **14**, 4689 (1981).
[9]J. Rossat-Mignod, P. Burlet, O. Vogt, and G. S. Landers, Ibid. **12**, 1101 (1979).
[10]J. Akimitsu, K. Siratori, G. Shirane, M. Iizumi, and T. Watanabe, J. Phys. Soc. Jpn. **44**, 172 (1978).
[11]A. Adam, D. Billerey, C. Terrier, R. Mainard, L. P. Regnault, J. Rossat-Mignod, and P. Meriel, Solid State Commun. **35**, 1 (1980); P. Day, M. W. Moore, C. Wilkinson, and R. R. A. Ziebeck, J. Phys. Ser. C **14**, 3423 (1981).
[12]K. Adachi, N. Achiwa, and M. Mekata, J. Phys. Soc. Jpn. **49**, 545 (1980).
[13]S. Funahashi, J. Hamaguchi, T. Tanaka, and E. Bannai, Solid State Commun. **23**, 859 (1977).
[14]P. Schobinger-Papamantellos, JMMM **28**, 97 (1982).
[15]T. Komatsubara, N. Sata, S. Kunii, I. Oguro, Y. Furukawa, Y. Onuki, and T. Kasuya, JMMM **31-34**, Pt. 1, 368 (1983).
[16]P. Burlet, J. Rossat-Mignod, J. M. Effantin, T. Kasuya, S. Kunii and T. Komatsubara, J. Appl. Phys. **53**, 2149 (1982).
[17]M. Takigawa, H. Yasuoka, T. Tanaka, Y. Ishizawa, M. Kasaya, and T. Kasuya, J. Magn. Magn. Mater. **31-34**, 1, 391 (1983).
[18]J. L. Soubeyroux, B. Buffat, N. Chevreau, and G. Demazeau, Physica B **120**, 227 (1983).
[19]W. C. Koehler in: Magnetic Properties of Rare Earth Metals, edited by R. J. Elliott, Plenum Press, NY (1972).
[20]M. Atoji, J. Chem. Phys. **48**, 560 (1968).
[21]M. Habenschuss, C. Stassis, S. K. Sinha, H. W. Deckman, and F. H. Spedding, Phys. Rev. B **10**, 1020 (1974).
[22]Y. Ishikawa, T. Komatsubara, and E. Hirahara, Phys. Rev. Lett. **23**, 532 (1969).
[23]Y. Shapira, J. Appl. Phys. **53**, 1914 (1982).
[24]S. A. Brazovskiĭ, I. E. Dzyaloshinskiĭ, and B. G. Kukharenko, Zh. Eksp. Teor. Fiz. **70**, 2257 (1976) [Sov. Phys. JETP **43**, 1178 (1976)].
[25]D. Mukamel and S. Krinsky, Phys. Rev. B **13**, 5065, 5078 (1976).

[26]I. E. Dzyaloshinskiĭ, Zh. Eksp. Teor. Fiz. **47**, 992 (1964) [Sov. Phys. JETP **20**, 665 (1964)].
[27]A. Michelson, Phys. Rev. B **16**, 577, 585, 5121 (1977).
[28]E. T. Whittacker and G. N. Watson, A Course of Modern Analysis, Cambridge Univ. Press, 1927. [Russ. Transl. Fizmatgiz, M., 1969].
[29]Yu. A. Izyumov, Zh. Eksp. Teor. Fiz. **42**, 1673 (1962) [Sov. Phys. JETP **15**, 1162 (1962)].
[30]Yu. A. Izyumov and V. M. Laptev, Zh. Eksp. Teor. Fiz. **85**, 2185 (1983) [Sov. Phys. JETP **58**, 1267 (1983)].
[31]V. A. Golovko and D. G. Sannikov, Zh. Eksp. Teor. Fiz. **82**, 959 (1982) [Sov. Phys. JETP **55**, 562 (1982)].
[32]Yu. A. Izyumov, V. M. Laptev, and S. B. Petrov, Fiz. Tverd. Tela **26**, 734 (1984) [Sov. Phys. Solid State **26**, 443 (1984)].
[33]N. N. Bogolyubov and Yu. A. Mitropol'skiĭ, Asimptoticheskie metody v teorii nelineĭnykh kolebaniĭ (Asymptotic Methods in the Theory of Nonlinear Oscillations), Nauka, 1974 [Engl. Transl. of earlier edition, Gordon and Breach, N.Y., 1964].
[34]K. P. Belov, Redkozemel'nye magnetiki i ikh primenenie (Rare-Earth Magnetic Materials and Their Applications), Nauka, M. 1980.
[35]O. V. Kovalev, Neprivodimye predstavleniya prostranstvennykh grupp Izd-vo Akad. Nauk USSR, Kiev (1961) [Engl. Transl. (Irreducible Representation of the Space Groups), Gordon and Breach, N.Y., 1965].
[36]Yu. A. Izyumov, V. M. Laptev, and S. B. Petrov, J. Magn. Magn. Mater. (1984).
[37]Yu. A. Izyumov, V. M. Laptev, and S. B. Petrov, Fiz. Met. Metalloved. **58** (1984).
[38]H. Pinto, M. Melamud, and E. Gurewitz, Acta Cryst. A **35**, 533 (1979).
[39]I. M. Vitebskiĭ, Zh. Eksp. Teor. Fiz. **82**, 357 (1982) [Sov. Phys. JETP **55**, 390 (1982)].
[40]V. G. Bar'yakhtar and I. M. Vitebskiĭ, "Effect of a field on inhomogeneous superconductors," (In Russian) Preprint ITF-83-24R, Kiev (1983).
[41]I. M. Vitebskiĭ, Fiz. Met. Metalloved. **55**, 468 (1983).
[42]A. I. Larkin and S. A. Pikin, Zh. Eksp. Teor. Fiz. **56**, 1664 (1969) [Sov. Phys. JETP **29**, 891 (1969)].
[43]J. Baruchel, A. Drillat, D. Fort, D. W. Jones, S. B. Palmer, and M. Schlenker, J. Magn. Magn. Mater **31**, 183 (1983).
[44]V. L. Pokrovsky, J. Phys. (Paris) **42**, 761 (1981).
[45]L. N. Bulaevskiĭ and D. I. Khomskiĭ, Zh. Eksp. Teor. Fiz. **74**, 1863 (1978) [Sov. Phys. JETP **47**, 971 (1978)].
[46]V. L. Pokrovskiĭ and A. A. Talapov, Zh. Eksp. Teor. Fiz. **75**, 1151 (1978) [Sov. Phys. JETP **48**, 579 (1978)].
[47]V. A. Golovko and A. P. Levanyuk, Zh. Eksp. Teor. Fiz. **81**, 2296 (1981) [Sov. Phys. JETP **54**, 1217 (1981)].
[48]J. Rossat-Mignod, P. Burlet, J. Villain, H. Bartholin, Tcheng-Si Wang, D. Florence, and O. Vogt, Phys. Rev. B **16**, 440 (1977).
[49]G. Meier, P. Fischer, W. Halg, B. Lebech, B. D. Rainford, and O. J. Vogt, J. Phys. C **11**, 1172 (1978).
[50]P. Fischer, B. Lebech, G. Meier, B. Rainford, and O. Vogt, Ibid., p. 345.
[51]G. Meier, P. Fischer, W. Halg, B. Lebech, B. D. Rainford, and O. Vogt, Ibid., p. 1173.
[52]H. Bartholin, D. Florence, Si-Tcheng Wang, and O. Vogt, Phys. Status Solidi **24**, 631 (1974).
[53]H. Bartholin, P. Burlet, S. Quezel, J. Rossat-Mignod, and O. Vogt, J. Phys. (Paris) **40**, Colloq. C5, 130 (1979).
[54]M. E. Fisher and W. Selke, Phys. Rev. Lett. **44**, 1502 (1980).
[55]V. L. Pokrovskiĭ and G. V. Uĭmin, Zh. Eksp. Teor. Fiz. **82**, 1640 (1982) [Sov. Phys. JETP **55**, 950 (1982)].
[56]E. L. Nagaev, Usp. Fiz. Nauk **136**, 61 (1982) [Sov. Phys. Usp. **25**, 31 (1982)].
[57]M. B. Walker, Phys. Rev. B **22**, 1338 (1980).
[58]V. S. Golovkin, V. N. Bykov, and V. A. Levdik, Metallofizika **2**, 48 (1980).
[59]J. Beille, J. Voiron, and M. Roth, Solid State Commun. **47**, 399 (1983).
[60]V. G. Bar'yakhtar and E. P. Stefanovskiĭ, Fiz. Tverd. Tela **11**, 1946 (1969) [Sov. Phys. Solid State **11**, 1566 (1970)].
[61]V. G. Bar'yakhtar and D. A. Yablonskiĭ, Fiz. Tverd. Tela **24**, 2522 (1982) [Sov. Phys. Solid State **24**, 1435 (1982)].

Translated by M. E. Alferieff